
OPTIMALITY-INFORMED NEURAL NETWORKS FOR SOLVING PARAMETRIC OPTIMIZATION PROBLEMS

Matthias K. Hoffmann

Saarland University,
Saarbrücken,
Germany

matthias.hoffmann@uni-saarland.de

Amine Othmane

Saarland University,
Saarbrücken,
Germany

Kathrin Flaßkamp

Saarland University,
Saarbrücken,
Germany

December 24, 2025

ABSTRACT

Many engineering tasks require solving families of nonlinear constrained optimization problems, parametrized in setting-specific variables. This is computationally demanding, particularly, if solutions have to be computed across strongly varying parameter values, e.g., in real-time control or for model-based design. Thus, we propose to learn the mapping from parameters to the primal optimal solutions and to their corresponding duals using neural networks, giving a dense estimation in contrast to gridded approaches. Our approach, Optimality-informed Neural Networks (OptINNs), combines (i) a KKT-residual loss that penalizes violations of the first-order optimality conditions under standard constraint qualifications assumptions, and (ii) problem-specific output activations that enforce simple inequality constraints (e.g., box-type/positivity) by construction. This design reduces data requirements, allows the prediction of dual variables, and improves feasibility and closeness to optimality compared to penalty-only training. Taking quadratic penalties as a baseline, since this approach has been previously proposed for the considered problem class in literature, our method simplifies hyperparameter tuning and attains tighter adherence to optimality conditions. We evaluate OptINNs on different nonlinear optimization problems ranging from low to high dimensions. On small problems, OptINNs match a quadratic-penalty baseline in primal accuracy while additionally predicting dual variables with low error. On larger problems, OptINNs achieve lower constraint violations and lower primal error compared to neural networks based on the quadratic-penalty method. These results suggest that embedding feasibility and optimality into the network architecture and loss can make learning-based surrogates more accurate, feasible, and data-efficient for parametric optimization.

Keywords Parametric Optimization · Nonlinear Optimization · Physics-Informed Neural Networks · Parametric Optimal Control · Semi-Supervised Learning

Acknowledgments

M. K. Hoffmann acknowledged funding by the German Research Foundation (DFG), Project No. 501928699. A. Othmane is grateful for the support from the German Federal Ministry of Research, Technology and Space, Project No. 05M22TSA.

1 Introduction

Many optimization problems which arise in engineering applications are parametric, i.e., the cost criteria as well as the constraints depend on external parameters. In multi-objective optimization, for instance, any scalarization technique introduces a family of optimization problems, which is parametrized via weights or alternative hyperparameters modeling prioritization among multiple objectives (Marler and Arora 2004). Parametric optimization problems also

show up in model-predictive control, in which subsequent optimal control problems vary in their current initial state, which contributes to the set of constraints (Bemporad et al. 2002). In general, many types of external influences from varying environmental conditions can be modeled as a vector of parameters entering the constraints and the objective of an optimization problem as presented by works from economics (Markowitz 1952) to engineering (Martins and Ning 2021). A historical review of parametric optimization can be found in (Oberdieck et al. 2016). For families of nonlinear restricted optimization problems, one is interested in finding not just the solutions for a small amount of parameter values, but the functional relationship between the problem instances and their respective optimal solutions. Under regularity assumptions, classical results guarantee that this relationship is, at least locally, a smooth curve (Fiacco 1983). Still, its computation raises numerical challenges, since a potentially high-dimensional, multivariate optimization problem cannot be solved to high accuracy on a dense parameter grid. Instead, a suitable representation for the curve of optimal solutions has to be found. To this aim, we propose a neural network (NN) representation and ensure approximation quality by a combined architecture and loss function design. This approach provides a parameter-to-optimal-solution mapping, which allows efficient evaluation as required in, e.g., optimization-based computer-aided design, decision-making in multi-objective optimization, or explicit model predictive control. Specifically, it provides a mapping for optimal primal-dual pairs, which are necessary for, e.g., sensitivity analysis (Rao and Papalambros 1989b). In safety-critical applications, where approximation errors of the NN model are intolerable, the solution can still serve as an initial guess for warm-starting any gradient-based optimization method.

1.1 Related Work

Solution maps for parametric optimization problems have classically been computed by pathfollowing and surrogate-based techniques. More recently, intensive research has been carried out for using neural network-based methods instead.

Pathfollowing methods Pathfollowing methods seek to update the solution when the parameter vector varies by computing a new solution from a given solution tuple via continuation (Guddat, Vazquez, and Jongen 1990). Continuation methods rely on the smoothness of the solution with respect to the parameters, as they use the implicit function theorem to predict the evolution of the optimal solution. For application to parametric optimization, the conditions of optimality are formulated as an implicit relation, allowing one to track the corresponding solution curve to compute a new estimate (Rao and Papalambros 1989a). A common approach is a predictor-corrector algorithm, which follows the tangent of the current solution and then re-enters the solution curve via Newton’s method. Detailed insights into the realization of this tracking are provided in (Allgower and Georg 1990). While the continuation path is uniquely defined in one-dimensional parameter spaces, the lack of a natural continuation direction complicates the tracking process in higher dimensions (Rheinboldt 1988). Such multiparametric optimization problems arise in optimal control problems with parametric initial conditions or multi-objective optimization problems with three or more objectives. These can be solved by pre-defining a path parameterized in arc-length to reduce the dimensionality to one, or by tracking the full manifold (Rheinboldt 1988). These methods, however, can be computationally intensive, which is a limitation for real-time applications, and give no dense representation of the solution curve.

Surrogate-based methods Distinct from pathfollowing, surrogate-based methods aim to find surrogate models for the mapping from parameters to the optimal solutions. In the context of optimal control with linear-quadratic cost and linear dynamics, the solution can be represented by a continuous, piecewise affine mapping as a function of the initial condition (Bemporad et al. 2002). Notably, only one sample of optimal solutions per combination of inequality constraints is sufficient to construct this mapping. In general, however, the structure of the solution mapping is unknown, creating a need for more versatile approximation methods. In (De Marchi et al. 2023), this broader scope is addressed by inferring the solution mapping without assuming a specific functional form. This motivates their use of surrogate models fitted via residual minimization of the KKT conditions. Minimizing residuals is analogous to performing root-finding on the KKT conditions, as it is done in Primal-Dual Interior Point methods (Boyd and Vandenberghe 2004). (De Marchi et al. 2023) proposes fitting a linear combination of Radial Basis Functions (RBFs) without using data samples by evaluating the residuals on a fixed grid of parameter values. These two approaches represent contrasting paradigms: the former leverages specific structural properties and data samples for control tasks, while the latter offers a general, grid-based framework that operates purely on residuals without incorporating solution data. However, the reliance on a predefined sample grid for the RBF limits the scalability of the latter approach. Specifically, RBF methods are more susceptible to the curse of dimensionality than neural networks, as the number of basis functions required to cover the space grows exponentially with the dimension (Bengio, Delalleau, and Roux 2005; Barron 1993).

Neural-network-based methods for parametric optimization problems Neural networks have seen significant advancements over the past two decades, with growing impact in engineering applications. Their ability to model complex, nonlinear relationships such as dynamic system behavior (Chen et al. 2018) and to process large datasets

makes them well-suited for tasks like predictive maintenance (Rivas et al. 2020). However, their requirement for large amounts of training data has long been a limiting factor, also when applying them to parametric optimization problems.

Early investigations primarily concentrated on developing recurrent neural networks or general differential equations designed to converge to local optima. In 1985, Hopfield demonstrated that Hopfield networks could minimize quadratic energy functions to address optimization problems, effectively estimating low-cost solutions to the Traveling Salesman Problem (Hopfield and Tank 1985). Building on this, Dhingra and Rao introduced mechanisms to handle constraints via penalty terms, approximating solutions for constrained optimization problems in mechanical engineering (Dhingra and Rao 1992). Similar approaches were explored in (Lillo et al. 1993). Zhang and Constantinides introduced Lagrange Programming Neural Networks by integrating the Karush-Kuhn-Tucker (KKT) conditions to address necessary conditions of optimality (Zhang and Constantinides 1992). Their resulting ordinary differential equation applied gradient descent on the primal and gradient ascent on the dual variables simultaneously by applying numerical integration methods. Wu and Tam specialized these methodologies for quadratic optimization problems (Wu and Tam 1999).

More recently, multi-layer perceptrons (MLPs) have become the predominant architecture for neural-network-based optimization. Nikbakht et al. proposed minimizing the Lagrangian directly by approximating the Lagrange multipliers through cross-validation (Nikbakht, Jonsson, and Lozano 2020). Liu et al. proposed training strategies that replicate the behavior of classical iterative optimizers, minimizing the cost function while incorporating constraints as penalty terms (Liu et al. 2024). Seo et al. demonstrated the use of Physics-Informed Neural Networks (PINNs) for classical optimization tasks, embedding constraints into the loss via penalty terms to achieve near-optimal results for optimal control problems (Seo 2024). Although quadratic-penalty methods are widely used, they are often considered suboptimal in modern optimization theory due to their tendency to produce solutions outside the feasible space (Lange 2013; Nocedal and Wright 2006). By relying on constraint-penalizing losses, these approaches do not fully exploit fundamental principles from optimization theory. In particular, they cannot provide Lagrange multipliers, which are helpful, e.g., as initial guesses for classical solvers, or even required, such as for sensitivity analysis (Rao and Papalambros 1989b).

Theory-informed neural networks To overcome the issue of requiring a large amount of data in the training of NN, theory-informed approaches have been developed. A foundational example was proposed by Munos, Baird, and Moore, who used NNs to approximate solutions to the Hamilton-Jacobi-Bellman (HJB) equation (Munos, Baird, and Moore 1999). For optimal control, this equation describes the necessary and sufficient conditions of optimality, and training is performed by minimizing its residuals. Similar approaches for solving the HJB-equation appear in other works (Cheng, Lewis, and Abu-Khalaf 2005; Izzo, Öztürk, and Märten 2019; Sirignano and Spiliopoulos 2018; Verma et al. 2024). Complementary to HJB-based methods, Effati and Pakdaman incorporate the Pontryagin Maximum Principle (PMP) to provide necessary conditions for controlling a dynamical system (Effati and Pakdaman 2013). Recent work by Nakamura-Zimmerer et al. exemplifies hybrid approaches, combining PMP-based data generation with HJB residual penalties (Nakamura-Zimmerer, Gong, and Kang 2021). In this framework, we see an opportunity to leverage the Karush-Kuhn-Tucker (KKT) conditions, which provide necessary conditions for optimality in constrained optimization problems.

1.2 Contributions of this paper

Addressing the challenges of aforementioned classical, surrogate-based and neural-network-based methods for parametric optimization problems, we propose *Optimality-Informed Neural Networks* (OptINNs) as a novel framework, in which optimality conditions are directly embedded into the training process and integrated in the design of the network’s architecture. This work is situated within the growing field of theory-informed machine learning, building on approaches such as PINNs for solving ordinary or partial differential equations (ODEs/PDEs), see (Raissi, Perdikaris, and Karniadakis 2019) or geometry-informed neural networks, see (Berzins et al. 2024). Similar to other surrogate-based approaches, neural networks allow for a dense representation of the solution space, while suffering less from the curse of dimensionality than kernel-based approaches (Bengio, Delalleau, and Roux 2005; Barron 1993). In contrast to methods based on the penalty method, incorporating optimality in the training allows for the estimation of the corresponding Lagrange multipliers.

For OptINNs, we propose a scheme that integrates data from optimal solutions with evaluations of optimality residuals, with respect to the KKT conditions, at sampled parameter instances. The scheme remains applicable even when no data from optimal solutions are available. Thereby, the method balances between a pure data-based training and the approach suggested in (De Marchi et al. 2023) for approximating the solution mapping of parameterized optimization problems. By framing our approach within the theory-informed machine learning paradigm, we benefit from utilizing established training strategies, (Wang et al. 2023; Krishnapriyan et al. 2021). We derive advantages of OptINNs in comparison to the established quadratic-penalty method: OptINNs do not show the known shortcoming of quadratic-penalty methods, which suffer from offsets in optimal solutions due to the designed constraint penalization. Unlike

quadratic-penalty-method-based neural networks, OptINNs predict both the primal and dual variables of parametrized optimal solutions. Despite this added task, numerical experiments demonstrate that same-sized OptINNs show little to no deterioration in performance or accuracy in small optimization problems as well as better performance and accuracy in larger optimal control problems.

1.3 Outline

The rest of this paper is structured as follows. In Section 2, the foundations of parametric nonlinear optimization, including the conditions of optimality, the local existence of solution mappings, and the construction of primal-dual patched solutions are laid. In Section 3, we present our main contributions. Namely, we discuss the design of loss functions incorporating optimality conditions and data fitting. Further, we discuss the architecture of OptINNs and their training, in particular the balancing of different components in the loss function. Then, in Section 4, we briefly introduce neural network training via constraint-penalization and discuss its disadvantages compared to the OptINN approach. Section 5 presents numerical experiments on four optimization problems, for which we also compare OptINNs with quadratic-penalty-method-based neural networks. Our focus lies on low-data regimes, in particular. Finally, Section 6 summarizes our findings and outlines directions for future research.

1.4 Notation

In this work, vectors, matrices and vector-valued functions are denoted with bold symbols. We denote the i -th element of a vector $\mathbf{v} \in \mathbb{R}^n$ as v^i . Similarly, for a set of indices $\mathbb{I} \subseteq \{1, 2, \dots, n\}$ the corresponding entries are represented as $\mathbf{v}^{\mathbb{I}}$. Variables, transformed to fulfill boundary and box constraints by design, are denoted with over- and underline $\overline{\underline{x}}$. In optimization problem formulations, comparison operators (e.g., \leq) applied to vectors and scalars are interpreted as element-wise operations. For instance, $\mathbf{v} \leq \mathbf{y}$ for $\mathbf{x}, \mathbf{y} \in \mathbb{R}^n$ implies $v^i \leq y^i$ for all $i = 1, \dots, n$. With $\mathcal{C}^k(\mathbb{R}^a, \mathbb{R}^b)$ we denote the set of all k -times continuously differentiable, vector-valued functions from \mathbb{R}^a to \mathbb{R}^b , with $a, b \in \mathbb{N}_+$. The derivative of a scalar-valued function f with scalar argument is denoted with f' . The gradient w.r.t \mathbf{x} of a scalar-valued function with vectorial argument $f : \mathbf{x} \mapsto f(\mathbf{x})$ is denoted with $\nabla_{\mathbf{x}} f(\mathbf{x})$. Similarly, the Jacobian matrix w.r.t. \mathbf{x} is denoted as $J_{\mathbf{x}} f(\mathbf{x})$ and the partial derivative w.r.t. the i -th entry of \mathbf{x} is denoted as $\frac{\partial f}{\partial x^i}$.

2 Parametric nonlinear optimization problems

In this section, we present the foundations for the upcoming approximation of solutions of parametric nonlinear optimization problems. For this, we first summarize optimization theory, mainly adapted from (Nocedal and Wright 2006). Afterwards, we present the class of optimization problems we handle in this work.

We consider a nonlinear optimization problems of the form

$$\begin{aligned} \min_{\mathbf{x} \in \mathbb{R}^n} f(\mathbf{x}, \mathbf{p}) \\ \text{s.t. } \mathbf{g}(\mathbf{x}, \mathbf{p}) \leq 0, \\ \mathbf{h}(\mathbf{x}, \mathbf{p}) = 0, \end{aligned} \quad \text{OP}(\mathbf{p})$$

where $\mathbf{x} \in \mathbb{R}^{n_x}$ is the vector of decision variables, $f \in \mathcal{C}^2(\mathbb{R}^{n_x} \times \mathbb{R}^{n_p}, \mathbb{R})$ is the cost function to be minimized, $\mathbf{g} \in \mathcal{C}^2(\mathbb{R}^{n_x} \times \mathbb{R}^{n_p}, \mathbb{R}^{n_g})$ and $\mathbf{h} \in \mathcal{C}^2(\mathbb{R}^{n_x} \times \mathbb{R}^{n_p}, \mathbb{R}^{n_h})$ are the inequality and equality constraints, respectively. Each of these functions additionally depend on the parameter vector $\mathbf{p} \in \mathbb{R}^{n_p}$, making it a parametric optimization problem. This parameter vector contains all entities that can be specified in an exact problem setting, like values of physical constants, the weights in a weighted sum of cost functions, or initial conditions in optimal control. For each choice of $\mathbf{p} \in \mathbb{R}^{n_p}$, $\text{OP}(\mathbf{p})$ states a nonlinear restricted optimization problem. Let \mathbf{x}^* denote an optimal solution of $\text{OP}(\mathbf{p})$.

Among the different variants of *constraint qualifications*, we employ the linear independence constraint qualification (LICQ), which ensures that, for fixed \mathbf{p} , the gradients of the active inequality constraints, i.e. for $\mathbb{A} := \{i \mid \mathbf{g}^i(\mathbf{x}^*, \mathbf{p}) = 0\}$, and the gradients of the equality constraints,

$$\mathbb{E} = \{\nabla_{\mathbf{x}} \mathbf{g}^i(\mathbf{x}^*, \mathbf{p}) \mid i \in \mathbb{A}\} \cup \{\nabla_{\mathbf{x}} \mathbf{h}^j(\mathbf{x}^*, \mathbf{p}) \mid j = 1, \dots, n_h\}$$

are linearly independent, i.e. with the cardinality of \mathbb{E} denoted by $|\mathbb{E}|$,

$$\nexists \boldsymbol{\xi} \in \mathbb{R}^{|\mathbb{E}|}, \text{ such that } \sum_{i=1}^{|\mathbb{E}|} \xi^i \mathbb{E}^i(\mathbf{x}^*, \mathbf{p}) = 0. \quad (1)$$

That this, the linearized feasible directions characterize the tangent cone at \mathbf{x}^* , see (Nocedal and Wright 2006).

With Lagrange multipliers $\boldsymbol{\mu} \in \mathbb{R}^{n_g}$ and $\boldsymbol{\lambda} \in \mathbb{R}^{n_h}$, we define the parametric Lagrangian

$$L : \mathbb{R}^{n_x} \times \mathbb{R}^{n_h} \times \mathbb{R}^{n_g} \times \mathbb{R}^{n_p} \rightarrow \mathbb{R}$$

associated with OP(\mathbf{p}) by $L(\mathbf{x}, \boldsymbol{\lambda}, \boldsymbol{\mu}, \mathbf{p}) = f(\mathbf{x}, \mathbf{p}) + \boldsymbol{\lambda}^\top \mathbf{h}(\mathbf{x}, \mathbf{p}) + \boldsymbol{\mu}^\top \mathbf{g}(\mathbf{x}, \mathbf{p})$. For an optimal solution \mathbf{x}^* of OP(\mathbf{p}), with associated Lagrange multipliers $\boldsymbol{\lambda}^*, \boldsymbol{\mu}^*$ the necessary conditions for optimality are given by the KKT conditions

$$\begin{array}{llll} \text{Stationarity:} & \nabla_x L(\mathbf{x}^*, \boldsymbol{\lambda}^*, \boldsymbol{\mu}^*, \mathbf{p}) = 0 & (\text{Stat}) & \\ \text{Primal feasibility:} & \mathbf{g}(\mathbf{x}^*, \mathbf{p}) \leq 0 & (\text{FeasG}) & \\ & \mathbf{h}(\mathbf{x}^*, \mathbf{p}) = 0 & (\text{FeasH}) & \text{KKT}(\mathbf{p}) \\ \text{Dual feasibility:} & \boldsymbol{\mu}_i^* \geq 0 \quad \forall i \in \{1, \dots, n_g\} & & \\ \text{Complementary slackness:} & \boldsymbol{\mu}_i^* \mathbf{g}^i(\mathbf{x}^*, \mathbf{p}) = 0 \quad \forall i \in \{1, \dots, n_g\}. & (\text{CSI}) & \end{array}$$

Under LICQ, an optimal solution \mathbf{x}^* satisfies the KKT conditions. To ensure that a candidate solution is a local minimum, second-order sufficient conditions (SOSC) must be satisfied. Specifically, the Hessian of the Lagrangian $\nabla_{xx} L$ evaluated at the optimal solution has to be positive definite on the tangent space defined by the active inequality and equality constraints, that is

$$\forall \mathbf{s} \neq 0 \in \mathbb{R}^{n_x}, \text{ it holds } \mathbf{s}^\top \nabla_{xx} L(\mathbf{x}^*, \boldsymbol{\lambda}^*, \boldsymbol{\mu}^*, \mathbf{p}) \mathbf{s} \geq 0, \text{ if } \begin{bmatrix} J_x \mathbf{g}^{\mathbb{A}}(\mathbf{x}^*, \mathbf{p}) \\ J_x \mathbf{h}(\mathbf{x}^*, \mathbf{p}) \end{bmatrix} \mathbf{s} = 0. \quad (2)$$

For further details refer to (Nocedal and Wright 2006). Decision variables and Lagrange multipliers are often also referred to as primal and dual variables, respectively.

2.1 Local existence of smooth parametric primal-dual solutions

A classical result for parametric optimization problems is given in (Fiacco 1983), which assumes stronger regularity of the cost and constraint functions, as detailed in the assumption. In the following, a neighborhood for $b \in \mathbb{B} \subseteq \mathbb{R}^q$ (not necessarily centered around b) is denoted by $\mathfrak{N}_b \subset \mathbb{B}$.

Assumption 1. *Without loss of generality, let \mathbf{x}^* denote the optimal solution to OP(0), i.e. the optimization problem OP(\mathbf{p}) for $\mathbf{p} = 0$. Then, we make the following assumptions.*

- For any fixed $\bar{\mathbf{p}}$, $f(\cdot, \bar{\mathbf{p}})$, $\mathbf{g}(\cdot, \bar{\mathbf{p}})$, $\mathbf{h}(\cdot, \bar{\mathbf{p}})$ are globally twice continuously differentiable in their first argument.
- There exists a neighborhood $\mathfrak{N}_0 \subset \mathbb{R}^{n_p}$, such that $\mathbf{g}(\mathbf{x}^*, \cdot)$, $\mathbf{h}(\mathbf{x}^*, \cdot)$, $\nabla_x f(\mathbf{x}^*, \cdot)$, $\nabla_x \mathbf{g}^i(\mathbf{x}^*, \cdot)$, $\nabla_x \mathbf{h}^j(\mathbf{x}^*, \cdot)$, $i = 1, \dots, n_g$, $j = 1, \dots, n_h$, are locally once continuously differentiable in their second argument on \mathfrak{N}_0 .
- LICQ and SOSC, see (1) and (2), hold at $(\mathbf{x}^*, 0)$ with associated Lagrange multipliers $\boldsymbol{\lambda}^*$ and $\boldsymbol{\mu}^*$.
- The multipliers $\boldsymbol{\mu}^*$ satisfy strict complementary slackness, i.e. $\boldsymbol{\mu}_i^* > 0$ for all $i \in \{i \mid \mathbf{g}^i(\mathbf{x}^*, 0) = 0\}$.

Theorem 2.1. *Under Assumption 1 it holds for OP(\mathbf{p}) and its optimal solution \mathbf{x}^* that*

- \mathbf{x}^* is a locally isolated minimizer of OP(0) and the associated Lagrange multipliers $\boldsymbol{\lambda}^*, \boldsymbol{\mu}^*$ are unique,
- for all $\mathbf{p} \in \mathfrak{N}_0$, there exists a unique, once continuously differentiable function

$$\mathbf{y}^* : \mathbf{p} \mapsto (\mathbf{y}_x^*(\mathbf{p}), \mathbf{y}_\lambda^*(\mathbf{p}), \mathbf{y}_\mu^*(\mathbf{p})),$$

called the primal-dual solution, with $\mathbf{y}^*(0) = (\mathbf{x}^*, \boldsymbol{\lambda}^*, \boldsymbol{\mu}^*)$ and such that the SOSC for a local minimum of problem OP(\mathbf{p}) are satisfied. Hence, $\mathbf{y}_x^*(\mathbf{p})$ is a locally unique local minimum of problem OP(\mathbf{p}) with associated unique Lagrange multipliers $\mathbf{y}_\lambda^*(\mathbf{p}), \mathbf{y}_\mu^*(\mathbf{p})$,

- for all \mathbf{p} in \mathfrak{N}_0 , the set of active inequality constraints remains unchanged, strict complementary slackness holds, and the union of gradients of active inequality and equality constraints are linearly independent at $\mathbf{y}_x^*(\mathbf{p})$.

2.2 Patched primal-dual solution mappings

Note that Fiacco’s setting in Section 2.1 holds locally on a neighborhood around a nominal solution. On a global scale, parametric optimization problems are known to exhibit jumps in the decision variables and Lagrange multipliers, for example due to changes in the set of active inequality constraints (Guddat, Vazquez, and Jongen 1990). For this work, we restrict our application to optimization problems for which the number of non-smooth points in the primal-dual solution mapping $\mathbf{p} \mapsto \mathbf{y}^*(\mathbf{p})$ is finite. Then, everywhere else, $\mathbf{y}^*(\mathbf{p})$ is at least continuously differentiable.

The following conditions on parametric optimization problems are derived in order to guarantee that $\mathbf{p} \mapsto \mathbf{y}^*(\mathbf{p})$ is piecewise continuous. Then, we extend Fiacco’s setting of Theorem 2.1 to the case in which multiple individual solutions are known, so that a patched solution with finitely many jumps can be constructed.

Let $\bar{\mathcal{P}} \subset \mathbb{R}^{n_p}$ denote a closed region of interest for the parameter \mathbf{p} . Further, let $\pi_a(\mathbf{p}) = a - \mathbf{p}$ denote a shifting operator. Note that Theorem 2.1 considers the nominal solution for parameter value $\mathbf{p} = 0$. However, this is w.l.o.g., so if \mathbf{x}_i^* is the optimal solution to $\text{OP}(\mathbf{p}_i)$, it also is an optimal solution to $\text{OP}(\pi_{\mathbf{p}_i}(0))$. If Assumption 1 holds at \mathbf{p}_i , we can apply Theorem 2.1 to the shifted problem and receive the existence of a neighborhood $\mathfrak{N}_{\mathbf{p}_i}$.

Assumption 2. *Given a parametric optimization problem $\text{OP}(\mathbf{p})$ and region of interest $\bar{\mathcal{P}} \subset \mathbb{R}^{n_p}$, we assume that there exist finitely many parameter values $\mathbf{p}_0, \mathbf{p}_1, \dots, \mathbf{p}_M$, with $M < \infty$, such that Theorem 2.1 holds for all $\text{OP}(\pi_{\mathbf{p}_i}(0))$, $i = 0, 1, \dots, M$, and $\bar{\mathcal{P}} \subset \bigcup_{i=0}^M \mathfrak{N}_{\mathbf{p}_i}$, i.e. $\bar{\mathcal{P}}$ is covered by finitely many neighborhoods $\mathfrak{N}_{\mathbf{p}_i}$.*

The restrictiveness of Assumption 2 depends on the given problem instance. As mentioned above, active set changes are one reason that restrict the neighborhoods in which Theorem 2.1 holds. Practically, one would choose \mathbf{p}_i in each combination of active constraints and check for local regularity of cost and constraint functions. The size of the region of interest is an additional design parameter that can be chosen to reduce the minimally required number of parameters.

Definition 2.1. *Given a set of solution curves \mathbf{y}_i^* on $\mathfrak{N}_{\mathbf{p}_i}$, for $i = 0, \dots, M$, satisfying Assumption 2, we define a patched primal-dual solution mappings $\mathbf{y}^* : \bar{\mathcal{P}} \rightarrow \mathbb{R}^{n_x} \times \mathbb{R}^{n_g} \times \mathbb{R}^{n_h}$ by*

$$\mathbf{y}^*(\mathbf{p}) = \mathbf{y}_i^*(\mathbf{p}) \text{ with } i = \min\{j \in \{0, \dots, M\} \mid \mathbf{p} \in \mathfrak{N}_{\mathbf{p}_j}\}.$$

Lemma 2.1. *The patched solution is a well-defined function if, for any $\mathbf{p} \in \bar{\mathcal{P}}$ which lies in the intersection of two neighborhoods, i.e. $\mathbf{p} \in \mathfrak{N}_{\mathbf{p}_i} \cap \mathfrak{N}_{\mathbf{p}_j}$, $i \neq j$, $0 \leq i, j \leq M$, $\text{OP}(\mathbf{p})$ has a unique globally optimal solution.*

This follows by construction, since, on the intersection $\mathfrak{N}_{\mathbf{p}_i} \cap \mathfrak{N}_{\mathbf{p}_j}$, the two solution mappings $\mathbf{y}_i, \mathbf{y}_j$ have to coincide excluding the possibility of multiple optimal solutions. In case the optimal solutions on the intersection $\mathfrak{N}_{\mathbf{p}_i} \cap \mathfrak{N}_{\mathbf{p}_j}$ differ (e.g., because of multiple global or local optima), Definition 2.1 guarantees that the patched solution is piecewise continuously differentiable with finitely many jumps.

Theorem 2.2. *If a function \mathbf{y}^* , as defined in Definition 2.1, exists on $\bar{\mathcal{P}}$, and Assumption 2 holds, from Theorem 2.1, it follows that \mathbf{y}^* is piecewise \mathcal{C}^1 on $\bar{\mathcal{P}}$ with finitely many jumps in all components, i.e. in primal and dual variables.*

In the following, we focus on problem settings satisfying Assumption 2. This poses not only constraints on the choice of cost and constraint functions, but also on the chosen parameters $\mathbf{p}_0, \dots, \mathbf{p}_M$, for which the neighborhoods have to cover the region of interest $\bar{\mathcal{P}}$. In particular, optimal solutions at $\mathbf{p}_0, \dots, \mathbf{p}_M$ will be required as training data in the learning approach. This defines the setting in which we propose the approximation of optimal solution mappings via optimality information.

3 Optimality-Informed Neural Networks

We introduce Optimality-informed neural networks (OptINNs) as a class of theory-informed neural networks that incorporate optimality conditions into the training process by designing a loss function based on the KKT conditions. Moreover, some problem constraints are directly transferred into a suitable architectural design of the network. Figure 1 provides a schematic overview of the full pipeline.

Given a parametric optimization problem of the form $\text{OP}(\mathbf{p})$ and a finite set $\{\mathbf{y}^*(\mathbf{p}_i)\}_{i=0}^M$ of solutions for the given parameters $\mathbf{p}_0, \dots, \mathbf{p}_M$ with $0 \leq M < \infty$, we aim for approximating the mapping \mathbf{y}^* of the parameterized problem for all $\mathbf{p} \in \bar{\mathcal{P}}$ as defined in Section 2.2. Our approach is to combine classical nonlinear optimization with deep learning. More concretely, we aim for approximating the mapping by a function parameterized in $\boldsymbol{\theta} \in \mathbb{R}^{n_\theta}$

$$\begin{aligned} \mathcal{N} : \mathbb{R}^{n_p} \times \mathbb{R}^{n_\theta} &\rightarrow \mathbb{R}^{n_y} = \mathbb{R}^{n_x + n_h + n_g} \\ (\mathbf{p}, \boldsymbol{\theta}) &\mapsto \mathcal{N}(\mathbf{p}, \boldsymbol{\theta}) = (\mathcal{N}_x^\top(\mathbf{p}, \boldsymbol{\theta}), \mathcal{N}_\lambda^\top(\mathbf{p}, \boldsymbol{\theta}), \mathcal{N}_\mu^\top(\mathbf{p}, \boldsymbol{\theta}))^\top, \end{aligned} \quad (3)$$

where $\mathcal{N}(\mathbf{p}, \boldsymbol{\theta})$ is decomposed into $\mathcal{N}_x(\mathbf{p}, \boldsymbol{\theta})$ for approximating the optimal primal solution mapping $\mathbf{y}_x^*(\mathbf{p})$, $\mathcal{N}_\lambda(\mathbf{p}, \boldsymbol{\theta})$ and $\mathcal{N}_\mu(\mathbf{p}, \boldsymbol{\theta})$ for the optimal dual solution mappings $\mathbf{y}_\lambda^*(\mathbf{p}, \boldsymbol{\theta})$ and $\mathbf{y}_\mu^*(\mathbf{p}, \boldsymbol{\theta})$, respectively. We design the loss function as a convex combination of two terms,

$$\mathcal{L}(\boldsymbol{\theta}; \alpha) = \alpha \mathcal{L}^{\text{KKT}}(\boldsymbol{\theta}) + (1 - \alpha) \mathcal{L}^{\text{MSE}}(\boldsymbol{\theta}) \quad (4)$$

with $\alpha \in [0, 1]$. The mean squared error (MSE) loss, \mathcal{L}^{MSE} , is the standard data-based loss for regression problems. It aggregates the pointwise error metric \mathcal{D}^{MSE} across all samples, where a single sample \mathbf{y} is compared with an estimate $\hat{\mathbf{y}}$:

$$\mathcal{L}^{\text{MSE}}(\boldsymbol{\theta}) = \sum_{i=0}^M \mathcal{D}^{\text{MSE}}(\mathcal{N}(\mathbf{p}_i, \boldsymbol{\theta}), \mathbf{y}^*(\mathbf{p}_i)), \quad \text{with} \quad \mathcal{D}^{\text{MSE}}(\hat{\mathbf{y}}, \mathbf{y}) = \|\hat{\mathbf{y}} - \mathbf{y}\|_2^2.$$

The term \mathcal{L}^{KKT} encodes optimality information, as described below. For $\alpha = 0$, we recover the pure regression problem whereas for $\alpha = 1$, the parameter identification replaces the classical nonlinear optimization, i.e. zero-finding of KKT conditions. For $M = 0$, i.e. no optimal solutions are available, \mathcal{L}^{MSE} vanishes independent of α , but the approach can still be applied as for $\alpha = 1$.

3.1 Optimality-informed design of loss functions

To embed conditions of optimality into the training process, we construct a loss function based on the Karush-Kuhn-Tucker conditions, see $\text{KKT}(\mathbf{p})$. Recall that the KKT conditions are either inequality or equality constraints, so we can interpret a deviation from equality constraints as a measure for optimality of the candidate solution. For the inequality constraints \mathbf{g} , we make use of the rectified linear unit $\text{ReLU} : \mathbb{R} \rightarrow \mathbb{R}, \mathbf{x} \mapsto \max(0, \mathbf{x})$ to only penalize violations of the inequality, i.e. penalize $\mathbf{g}(\mathbf{x}, \mathbf{p}) > 0$. Non-negativity of the Lagrange multiplier $\boldsymbol{\mu}$ is guaranteed by architectural design, as discussed in Section 3.2.

Definition 3.1 (Unimodal Penalty Function). *A continuous function $\phi : \mathbb{R} \rightarrow [0, \infty)$ is called a unimodal penalty function if $\phi(0) = 0$, ϕ is differentiable on $\mathbb{R} \setminus \{0\}$, and $x\phi'(x) > 0$ for all $x \neq 0$.*

Examples for unimodal penalty functions are the absolute value function or the square function.

With unimodal penalty functions P^i , $i \in \mathcal{T} = \{\text{Stat}, \text{FeasG}, \text{FeasH}, \text{CSl}\}$, for a given point $(\mathbf{x}, \boldsymbol{\lambda}, \boldsymbol{\mu})$ and associated parameter \mathbf{p} , we can formulate deviations from the KKT conditions $\text{KKT}(\mathbf{p})$ as

$$\begin{aligned} \mathcal{D}^{\text{Stat}}(\mathbf{x}, \boldsymbol{\lambda}, \boldsymbol{\mu}, \mathbf{p}) &= \frac{1}{n_x} \sum_{i=1}^n P^{\text{Stat}} \left(\frac{\partial L}{\partial \mathbf{x}^i}(\mathbf{x}, \boldsymbol{\lambda}, \boldsymbol{\mu}, \mathbf{p}) \right), & \mathcal{D}^{\text{FeasG}}(\mathbf{x}, \mathbf{p}) &= \frac{1}{n_g} \sum_{i=1}^{n_g} P^{\text{FeasG}}(\text{ReLU}(\mathbf{g}^i(\mathbf{x}, \mathbf{p}))), \\ \mathcal{D}^{\text{CSl}}(\mathbf{x}, \boldsymbol{\mu}, \mathbf{p}) &= \frac{1}{n_g} \sum_{i=1}^{n_g} P^{\text{CSl}}(\boldsymbol{\mu}^i \mathbf{g}^i(\mathbf{x}, \mathbf{p})), & \mathcal{D}^{\text{FeasH}}(\mathbf{x}, \mathbf{p}) &= \frac{1}{n_h} \sum_{i=1}^{n_h} P^{\text{FeasH}}(\mathbf{h}^i(\mathbf{x}, \mathbf{p})). \end{aligned}$$

We sample a set of parameters $\{\mathbf{p}_i\}_{i=1}^N$ from a uniform distribution \mathcal{U} with lower and upper bounds $\underline{\mathbf{p}}$ and $\bar{\mathbf{p}}$. Using the neural network \mathcal{N} parametrized by $\boldsymbol{\theta}$ (cf. (3)), we predict the corresponding primal and dual variables for these samples. Averaging the deviations from the KKT conditions over this set yields the functions

$$\begin{aligned} \mathcal{L}^{\text{Stat}}(\boldsymbol{\theta}) &= \frac{1}{N} \sum_{i=1}^N \mathcal{D}^{\text{Stat}}(\mathcal{N}_x(\mathbf{p}_i, \boldsymbol{\theta}), \mathcal{N}_\lambda(\mathbf{p}_i, \boldsymbol{\theta}), \mathcal{N}_\mu(\mathbf{p}_i, \boldsymbol{\theta}), \mathbf{p}_i), & \mathcal{L}^{\text{FeasG}}(\boldsymbol{\theta}) &= \frac{1}{N} \sum_{i=1}^N \mathcal{D}^{\text{FeasG}}(\mathcal{N}_x(\mathbf{p}_i, \boldsymbol{\theta}), \mathbf{p}_i), \\ \mathcal{L}^{\text{CSl}}(\boldsymbol{\theta}) &= \frac{1}{N} \sum_{i=1}^N \mathcal{D}^{\text{CSl}}(\mathcal{N}_x(\mathbf{p}_i, \boldsymbol{\theta}), \mathcal{N}_\mu(\mathbf{p}_i, \boldsymbol{\theta}), \mathbf{p}_i), & \mathcal{L}^{\text{FeasH}}(\boldsymbol{\theta}) &= \frac{1}{N} \sum_{i=1}^N \mathcal{D}^{\text{FeasH}}(\mathcal{N}_x(\mathbf{p}_i, \boldsymbol{\theta}), \mathbf{p}_i). \end{aligned} \quad (5)$$

In the sequel, we refer to these functions as KKT-residuals. They serve as the basis for identifying the parameters $\boldsymbol{\theta}$ of the associated neural network \mathcal{N} . The weighted and summed KKT-residuals give the KKT-loss function

$$\mathcal{L}^{\text{KKT}}(\boldsymbol{\theta}) = \omega^{\text{Stat}} \mathcal{L}^{\text{Stat}}(\boldsymbol{\theta}) + \omega^{\text{FeasG}} \mathcal{L}^{\text{FeasG}}(\boldsymbol{\theta}) + \omega^{\text{FeasH}} \mathcal{L}^{\text{FeasH}}(\boldsymbol{\theta}) + \omega^{\text{CSl}} \mathcal{L}^{\text{CSl}}(\boldsymbol{\theta}) \quad (6)$$

that combines the weighted deviations of the model predictions for all KKT-residuals. The weights ω^i , $i \in \mathcal{T}$, are used for balancing the different loss terms, their tuning will be explained in Section 3.3.2. Next, we show that only KKT-points, combinations of primal and dual variables satisfying the KKT conditions, produce a loss value of zero.

Lemma 3.1 (Zero KKT-loss for KKT-points). *Given an optimization problem of the form $\text{OP}(\mathbf{p})$ with parameter $\mathbf{p} \in \mathbb{R}^{n_p}$, primal and dual variables $(\mathbf{x}^*, \boldsymbol{\lambda}^*, \boldsymbol{\mu}^*) \in \mathbb{R}^{n_x} \times \mathbb{R}^{n_h} \times \mathbb{R}_{\geq 0}^{n_g}$, the KKT-residuals (5) with corresponding unimodal penalty functions P^i , $i \in \mathcal{T}$, are zero, i.e.*

$$\mathcal{D}^{\text{Stat}}(\mathbf{x}^*, \boldsymbol{\lambda}^*, \boldsymbol{\mu}^*, \mathbf{p}) = \mathcal{D}^{\text{FeasG}}(\mathbf{x}^*, \mathbf{p}) = \mathcal{D}^{\text{FeasH}}(\mathbf{x}^*, \mathbf{p}) = \mathcal{D}^{\text{CSl}}(\mathbf{x}^*, \boldsymbol{\mu}^*, \mathbf{p}) = 0,$$

if and only if $(\mathbf{x}^*, \boldsymbol{\lambda}^*, \boldsymbol{\mu}^*)$ and \mathbf{p} satisfy $\text{KKT}(\mathbf{p})$.

Proof. See Appendix B. □

3.2 Optimality-informed architecture

A comparison of the KKT-conditions with the formulated penalties shows that we have not included a penalty for the dual feasibility, cf. $\text{KKT}(\mathbf{p})$ and (5). We specifically did not include this as a penalty, as it can be fulfilled by architectural design. The architecture used in our experiments is based on a standard MLP. An MLP is the repeated composition of linear-affine transformations, defined by weight matrices $\mathbf{W}^{(l)} \in \mathbb{R}^{u_l \times u_{l-1}}$ and bias vectors $\mathbf{b}^{(l)} \in \mathbb{R}^{u_l}$, and nonlinear activation functions $\mathbf{a}^{(l)} : \mathbb{R}^{u_l} \rightarrow \mathbb{R}^{u_l}$. The entries of all $\mathbf{W}^{(l)}$ and $\mathbf{b}^{(l)}$ form the parameter vector $\boldsymbol{\theta}$. In our setting, the resulting MLP $\mathcal{N} : \mathbb{R}^{n_p} \times \mathbb{R}^{n_\theta} \rightarrow \mathbb{R}^{n_y}$ with L layers is given as $\mathcal{N}(\mathbf{p}, \boldsymbol{\theta}) := \boldsymbol{\nu}^{(L)}(\mathbf{p})$ with

$$\begin{aligned} \boldsymbol{\nu}^{(0)} &= \mathbf{p}, \\ \mathbf{z}^{(l)} &= \mathbf{W}^{(l)} \boldsymbol{\nu}^{(l-1)} + \mathbf{b}^{(l)} \quad \forall l \in \{1, \dots, L\}, \\ \boldsymbol{\nu}^{(l)} &= \mathbf{a}^{(l)}(\mathbf{z}^{(l)}) \quad \forall l \in \{1, \dots, L\}. \end{aligned}$$

To enforce dual feasibility, the components of $\mathbf{z}^{(L)}$ associated with the dual variables of inequality constraints are transformed in the final activation layer $\mathbf{a}^{(L)}$ via the Softplus function

$$\text{Softplus} : \mathbb{R} \rightarrow (0, \infty), \quad x \mapsto \ln(1 + e^x),$$

so that the resulting output satisfies this condition (see $\text{KKT}(\mathbf{p})$).

Remark 3.1. *If some of the inequality constraints in $\text{OP}(\mathbf{p})$ are of the form $x \leq \bar{x}$, $\underline{x} \leq x$, or $\underline{x} \leq x \leq \bar{x}$, i.e. lower bounds, upper bounds, or box constraints, these can be fulfilled by design as well. To enforce feasibility of the predicted decision variables directly through the network architecture, we apply suitable activation functions tailored to the type of constraint. Lower bounds and upper bounds are fulfilled by $\underline{x} = \underline{x} + \text{Softplus}(x)$ and $\bar{x} = \bar{x} - \text{Softplus}(x)$, respectively. For box constraints, the sigmoid function $\sigma : \mathbb{R} \rightarrow (0, 1)$, $x \mapsto \frac{1}{1+e^{-x}}$ is shifted and scaled such that $\bar{x} = \underline{x} + (\bar{x} - \underline{x})\sigma(x) \in (\underline{x}, \bar{x})$.*

Concatenating these transformations for bound- and box-constrained decision variables with identity mappings for unconstrained variables and the softplus function for dual variables to inequality constraints gives a vector-valued function forming the final nonlinear activation layer $\mathbf{a}^{(L)}$. Since boundary and box-constraints are now always satisfied, their contributions to $\mathcal{L}^{\text{FeasG}}(\boldsymbol{\theta})$ are always 0.

3.3 OptINN training

From the PINN literature, mainly from (Wang et al. 2023) for this work, some key insights for training theory-informed neural networks can be drawn. Here, we summarize the methods used for this work’s numerical results.

3.3.1 Tuning the data loss and optimality trade-off

As introduced previously, the parameter α tunes the trade-off between \mathcal{L}^{MSE} and \mathcal{L}^{KKT} . While our main focus is the minimization of \mathcal{L}^{KKT} , the topologies of the \mathcal{D}^i , $i \in \mathcal{T}$, can, depending on the optimization problem, be multimodal and as such much more involved compared to the convex \mathcal{D}^{MSE} , see for example (Krishnapriyan et al. 2021). Thus, we divide training into three phases:

1. initialization phase of length d^{init} : α is kept constant at its lowest value $\underline{\alpha}$
2. annealing phase of length d^{anneal} : α is increased following a cosine function
3. finalization phase of length d^{final} : α is kept at its highest value $\bar{\alpha}$.

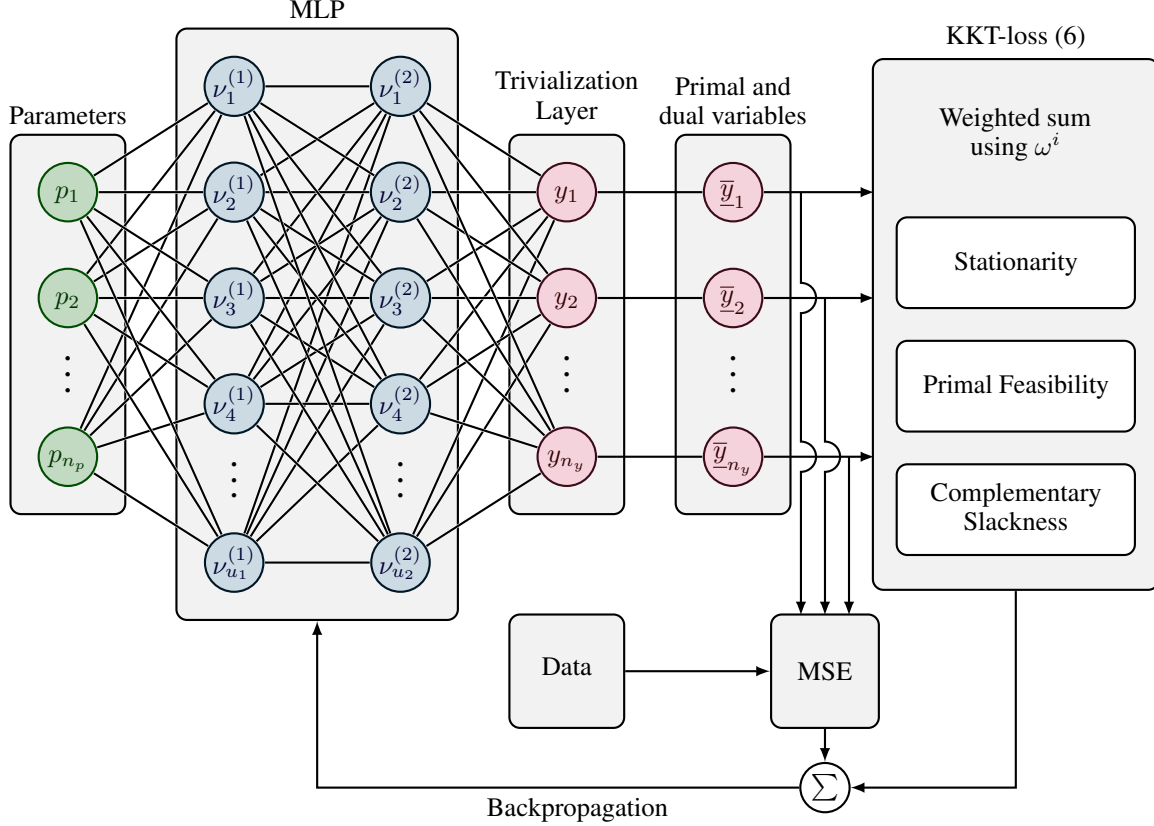


Figure 1 The architecture and training of a 4-layer OptINN. The problem parameters are passed through the MLP for the given parameter vector \mathbf{p} . The trivialization layer includes all bound and box constraints on the output variables, giving the variables marked with $\overline{(\cdot)}$. The output $\overline{\mathbf{y}} \in \mathbb{R}^{n_y}$ corresponds to the concatenation of the primal variables \mathbf{x} and dual variables $\boldsymbol{\mu}$ and $\boldsymbol{\lambda}$

For the epoch d , where an epoch refers to one complete pass through the entire training dataset by the learning algorithm,

$$\alpha(d) = \begin{cases} \underline{\alpha} & \text{if } d \leq d^{\text{init}} \\ \underline{\alpha} + \frac{1}{2}(\overline{\alpha} - \underline{\alpha})(1 - \cos(\pi \frac{d-d^{\text{init}}}{d^{\text{anneal}}})) & \text{if } d^{\text{init}} < d \leq d^{\text{init}} + d^{\text{anneal}} \\ \overline{\alpha} & \text{if } d^{\text{init}} + d^{\text{anneal}} \leq d \leq d^{\text{init}} + d^{\text{anneal}} + d^{\text{final}} \end{cases} .$$

This progression allows the convex MSE-loss to guide early training, while gradually shifting focus to the KKT-loss function. Figure 2 shows one cycle for initialization and finalization phases of length 50, $\underline{\alpha} = 0.1$, and $\overline{\alpha} = 0.9$.

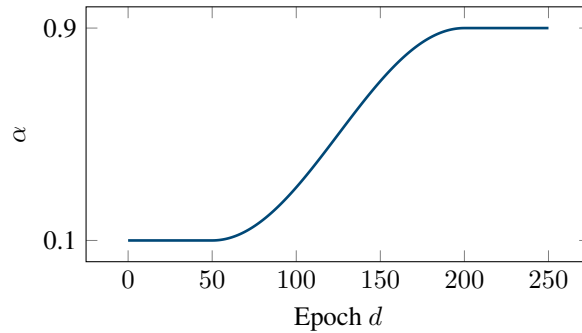


Figure 2 Cosine scheduling for α with $\underline{\alpha} = 0.1$, $\overline{\alpha} = 0.9$, and initialization and finalization phases of lengths $d^{\text{init}} = d^{\text{final}} = 50$ over 200 epochs

3.3.2 Loss balancing

Similar to PINNs, a key point in training OptINNs is the imbalance between the gradients of the different losses (Wang et al. 2023). During training, losses with larger gradients are prioritized in minimization, resulting in a potential deterioration of other losses. To handle this, automated loss balancing has been introduced for scaling the different costs in such a way that the resulting descent direction lies in the cone of common descent for all losses. In (Wang et al. 2023) two methods, one based on the so-called neural tangent kernel matrix and one based on the gradients of loss functions, are summarized. Employing the second approach, the weights ω^{Stat} , ω^{FeasG} , ω^{FeasH} , and ω^{CSI} (6) are set according to the magnitude of the gradients with respect to the MLP’s parameters θ with

$$\omega^i = \begin{cases} \frac{\sum_{j \in \mathcal{T}} \|\nabla_{\theta} \mathcal{L}^j(\theta)\|}{\|\nabla_{\theta} \mathcal{L}^i(\theta)\|} \quad \forall i \in \mathcal{T}, & \|\nabla_{\theta} \mathcal{L}^i(\theta)\| > \beta \\ 1, & \text{else} \end{cases}$$

for some small β .

Before we numerically validate the OptINN approach in detail, we present the variant based on the quadratic-penalty method, which is known from literature and serves as a baseline for the OptINN validation.

4 The KKT-loss function in comparison to constraint-penalization

Although the KKT-loss function introduces additional complexity, it offers significant advantages over the quadratic-penalty method, as discussed in this section. We begin by summarizing the classical quadratic-penalty method and the derived quadratic-penalty-method-based neural networks (PMNNs), highlighting the specific weaknesses the latter inherits. Subsequently, we compare PMNNs (using constraint-penalization) against OptINNs (using the KKT-loss). Our analysis demonstrates the superiority of the OptINN framework across three key aspects: (i) The integration of data-driven terms with the respective optimization losses, (ii) the suitability of each loss formulation for hyperparameter tuning, and (iii) the practical restrictions regarding validation and scheduling during training.

4.1 Quadratic-penalty-method-based neural networks

As discussed in Section 1.1, previous works (Lillo et al. 1993; Liu et al. 2024) employed the quadratic-penalty method to approximate the mapping $\mathbf{p} \mapsto \mathbf{x}^*(\mathbf{p})$ with MLPs $\mathcal{N}^{\text{PMNN}} : \mathbb{R}^{n_p} \times \mathbb{R}^{n_{\theta}} \rightarrow \mathbb{R}^{n_x}$. Given an optimization problem of the form $\text{OP}(\mathbf{p})$ the quadratic-penalty method combines the cost function and constraints into the constraint-penalizing loss

$$\mathcal{L}^{\text{PM}}(\theta) = \frac{1}{N} \sum_{i=1}^N \mathcal{D}^{\text{PM}}(\mathcal{N}^{\text{PMNN}}(\mathbf{p}, \theta), \gamma_g, \gamma_h, \mathbf{p}) \quad (7)$$

$$\mathcal{D}^{\text{PM}}(\mathbf{x}, \gamma_g, \gamma_h, \mathbf{p}) = f(\mathbf{x}, \mathbf{p}) + \gamma_g \sum_{i=1}^{n_g} \text{ReLU}(\mathbf{g}^i(\mathbf{x}, \mathbf{p}))^2 + \gamma_h \sum_{j=1}^{n_h} \mathbf{h}^j(\mathbf{x}, \mathbf{p})^2,$$

where γ_g and γ_h are tunable parameters, with higher values resulting in more focus on satisfying the constraint. Similar to OptINNs, this can be combined with an MSE-loss to incorporate training data by replacing \mathcal{L}^{KKT} in (4) with \mathcal{L}^{PM} .

One major problem of the constraint-penalizing loss is that it can only be used to compute the constrained optimum of $\text{OP}(\mathbf{p})$ if the unconstrained minimum of $f(\mathbf{x}, \mathbf{p})$ is feasible (Nocedal and Wright 2006). The following example illustrates this limitation.

Example 4.1. *For the equality constrained optimization problem*

$$\min_{\mathbf{x} \in \mathbb{R}^2} f(\mathbf{x}), \text{ s.t. } h(\mathbf{x}) = 0$$

the associated constraint-penalizing loss is $f(\mathbf{x}) + \gamma_h h(\mathbf{x})^2$. The corresponding condition of optimality is given by $\nabla_{\mathbf{x}} f(\mathbf{x}) + 2\gamma_h h(\mathbf{x}) \nabla_{\mathbf{x}} h(\mathbf{x}) = 0$, where $2\gamma_h h(\mathbf{x})$ can be interpreted as an estimate for the Lagrange multiplier λ . Since $h(\mathbf{x}) = 0$ for any feasible solution, this condition can only be satisfied if $\nabla_{\mathbf{x}} f(\mathbf{x}) = 0$, i.e. it can only find the constrained minimum when it coincides with the unconstrained minimum. Otherwise, the computed solution of the constraint-penalized problem will be infeasible for the original problem.

Also, if inequality constraints are present in addition, the quadratic-penalty-method might yield infeasible solutions. As a consequence, the minimizer and minimum value of $\mathcal{D}^{\text{PM}}(\mathbf{x}, \mu_g, \mu_h, \mathbf{p})$ vary with the choice of γ_g and γ_h . For a

concrete example, see Figure 3, where, with increasing γ_g , the minimizer and minimum of the constraint-penalizing loss shift towards the constrained optimum ($x = 1, f(x) = -1$) without reaching it.

In contrast, from the fact that all $\mathcal{P}^i, i \in \mathcal{T}$, are unimodal penalty functions, we can deduce that \mathcal{L}^{KKT} , see (6), is lower bounded by zero independent of the values $\omega^i, i \in \mathcal{T}$.

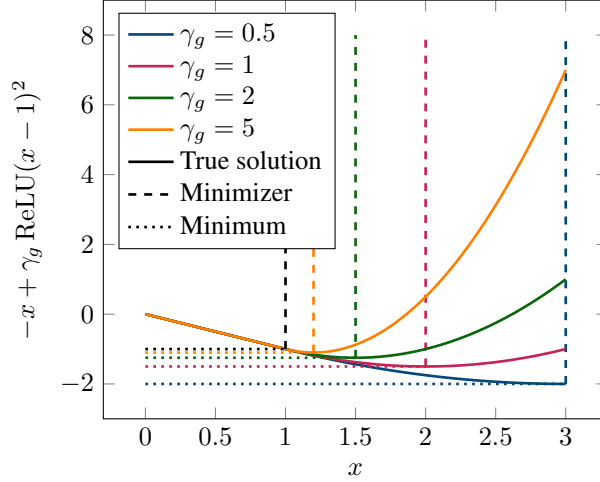


Figure 3 Minima of $-x + \gamma_g \text{ReLU}(x - 1)^2$ under changing γ_g for the optimization problem $\min_{x \in \mathbb{R}} -x$ s.t. $x \leq 1$. The dashed and dotted lines mark the corresponding minimizer and minimum, respectively. Increasing γ_g shifts the minimizer closer to the true optimum $x = 1$, but also increases the minimum. All suggested minimizer lie in the infeasible region $x > 1$

4.2 Alignment of Loss Minima with Training Data

Next, we discuss how well the loss minima align with training data, i.e. how well numerical optimizers' solutions minimize the losses. Numerical optimizers like IPOPT (Wächter and Biegler 2006) or WORHP (Büskens and Wassel 2013) directly aim to solve the KKT conditions. As a consequence, solutions computed with these solvers directly exhibit a KKT-loss close to 0. This implies that, for any given data point, the MSE-loss (based on numerical solver data) and the KKT-loss share the same optimum, within the limits of numerical solver's tolerances. From Section 4.1, it is evident that, since the constraint-penalizing loss predicts infeasible solutions for non-trivial cases, both losses, MSE and constraint-penalizing loss, will contradict each other. In such cases, the data-based MSE-loss guides the prediction towards the data points and the constraint-penalizing loss guides it to the minimum of $\mathcal{D}^{\text{PM}}(\mathbf{x}, \gamma_g, \gamma_h, \mathbf{p})$.

4.3 Evaluation metrics for hyperparameter tuning

The objective of hyperparameter tuning is to identify algorithmic parameters that yield optimal model performance according to an evaluation metric $\mathcal{D}^{\text{eval}} : \mathbb{R}^{n_\theta} \rightarrow \mathbb{R}$ (Bergstra et al. 2011). In neural network training, this typically entails tuning learning rates, batch sizes (see (Goodfellow, Bengio, and Courville 2016)), or loss function parameters such as $\underline{\alpha}, \bar{\alpha}, \gamma_g$, and γ_h by optimizing the trained performance. This process is formally a bilevel optimization problem

$$\begin{aligned} \min_{\mathbf{d}_{\text{hyper}}} \quad & \mathcal{D}^{\text{eval}}(\boldsymbol{\theta}^*) \\ \text{s.t.} \quad & \boldsymbol{\theta}^* = \mathcal{A}(\mathcal{L}_{\text{train}}, \mathbf{d}_{\text{hyper}}), \end{aligned}$$

where $\mathbf{d}_{\text{hyper}}$ denotes the full set of hyperparameters and \mathcal{A} represents the algorithm that minimizes the training loss $\mathcal{L}_{\text{train}}$. Note that $\mathbf{d}_{\text{hyper}}$ may influence both, the definition of $\mathcal{L}_{\text{train}}$ and the behavior of \mathcal{A} .

We now analyze the suitability of the KKT-loss versus the constraint-penalizing loss as the validation metric $\mathcal{D}^{\text{eval}}$. The KKT-loss is a robust choice for $\mathcal{D}^{\text{eval}}$ because its global minimum is zero, regardless of the hyperparameter values. In contrast, the constraint-penalizing loss is unsuitable for tuning the penalty weights γ_g and γ_h . As established previously, the constraint-penalizing lower bound is directly dependent on these weights. Since the penalty terms in (7) are non-negative, minimizing the constraint-penalizing loss with respect to $\mathbf{d}_{\text{hyper}}$ leads to the trivial solution where $\gamma_g, \gamma_h \rightarrow 0$ (or $-\infty$ if γ_g, γ_h are unconstrained). Consequently, one must rely on alternative strategies: either using a data-driven metric (e.g., MSE on validation data) or heuristically selecting γ_g and γ_h , balancing constraint satisfaction with training stability since large values result in increasing gradients.

4.4 Validation, scheduling, and early-stopping

Scheduling describes the active changing of hyperparameters during training, often in regard to previous training results, in order to achieve better performance or accelerate the training (Bishop and Bishop 2023). One example is the ReduceLROnPlateau learning rate scheduler that reduces the learning rate by a multiplicative factor once the validation loss hits a plateau and stops decreasing. Again, the lower-boundedness of the KKT-loss allows its application as a validation loss, whereas the constraint-penalizing loss is more restricted. When γ_g and γ_h are fixed for the whole training, employing it as a validation loss is possible since it is lower-bounded by its minimum, thus, disallowing tuning during training. When γ_g and γ_h are tuned during training, the constraint-penalizing loss does not exhibit the same lower bound for intermediate values of γ_g and γ_h , since it increases with rising γ_g and γ_h , see Figure 3. This may result in premature reduction of learning rate impairing the training. The same arguments hold when convergence is evaluated on the number of epochs without decreased loss, a technique referred to as early-stopping.

5 Numerical results

In this section, we collect numerical experiments for comparing OptINNs with PMNNs based on the quadratic penalty method (Liu et al. 2024). On four different optimization problems of increasing difficulty, we compare the resulting models based on constraint violation and the mean squared error in the primal variables only, since PMNNs are not able to give predictions for dual variables. The NNs were trained using PyTorch (Paszke et al. 2019), the training data of each problem was computed using IPOPT (Wächter and Biegler 2006) after formulation in CasADi (Andersson et al. 2019). The parameters of IPOPT describing accuracies were set to 10^{-12} to be close approximations of the true minimizers. For each problem, the hyperparameters were computed using the toolbox Optuna (Akiba et al. 2019) for 200 iterations by training OptINNs and PMNNs on three distinct seeds, where the average validation loss over these three trained networks is optimized for. As explained in Section 3.1, the hyperparameter tuning metric for the PMNNs cannot be the constraint-penalizing cost function. Still, to compare OptINNs with PMNNs of optimized hyperparameters, the metric for hyperparameter tuning is the mean squared error w.r.t. training data generated from 256 parameter values (input values) sampled from an equidistant grid. Since we want to compare low-data domains, for the training process, we fix the values γ_g and γ_h so that the constraint-penalizing loss can be used for validation. For OptINNs, the validation loss and hyperparameter tuning metric is computed as the KKT-loss, where $P^{\text{Stat}}(x) = P^{\text{FeasG}}(x) = P^{\text{FeasH}}(x) = P^{\text{CSl}}(x) = |x|$, not requiring any additional training data. The OptINN hyperparameters optimized for are summarized in Table 1. We grouped the penalty formulating functions to reduce the search space dimension and ensure that for $x \approx 0$ the fulfillment of constraints has at least the same priority as the stationarity condition and the complementary slackness. The PMNN implementation is chosen to follow the

Table 1 Overview of OptINN hyperparameters.

Category	Parameters / Configurations
Optimizer	Learning rate, Weight decay
Scheduling	Min/max trade-off ($\underline{\alpha}, \bar{\alpha}$), duration of initialization and annealing phases ($d^{\text{init}}, d^{\text{anneal}}$)
Sampling	Number of parameter samples N (per training/validation step)
Penalty Functions	<ol style="list-style-type: none"> 1. $P^{\text{Stat}} = P^{\text{CSl}} = P^{\text{FeasG}} = P^{\text{FeasH}} = x$ 2. $P^{\text{Stat}} = P^{\text{CSl}} = P^{\text{FeasG}} = P^{\text{FeasH}} = x^2$ 3. $P^{\text{Stat}} = P^{\text{CSl}} = x^2, P^{\text{FeasG}} = P^{\text{FeasH}} = x + x^2$ 4. $P^{\text{Stat}} = P^{\text{CSl}} = P^{\text{FeasG}} = P^{\text{FeasH}} = x + x^2$

literature (Liu et al. 2024; Lillo et al. 1993), resulting in the hyperparameters as given in Table 2. The computed

Table 2 Overview of PMNN hyperparameters.

Category	Parameters / Details
Optimizer	Learning rate, Weight decay set to 0 due to computed value being negligible
Loss Balancing	Trade-off parameter (Data loss vs. Constraint loss)
Constraint Weights	Weights for equality and inequality constraints
Sampling	Number of parameter samples N (per training/validation step)

hyperparameters were then evaluated on five more seeds. These five trainings are what we use for comparison in this section.

To ensure comparable expressivity, both OptINNs and PMNNs utilize MLPs with identical depth and uniform width across all hidden layers. The sole architectural distinction lies in the final output layer of the OptINN, which contains additional parameters for predicting dual variables. Structurally, each linear transformation is followed by layer normalization (Ba, Kiros, and Hinton 2016) and a ReLU activation. All parameters are optimized using AdamW (Loshchilov and Hutter 2019) with default settings.

The optimized hyperparameters for each problem are summarized in Appendix A. After training, the performance metrics, the MSE for the primal variables

$$\mathcal{L}^{\text{MSE,primal}}(\boldsymbol{\theta}) = \sum_{i=1}^N \left\| \mathbf{x}^{\star i} - \mathcal{N}_x(\mathbf{p}_i; \boldsymbol{\theta}) \right\|_2^2$$

and the absolute constraint violation

$$\mathcal{L}^{\text{ConstrViol}}(\boldsymbol{\theta}) = \sum_{i=1}^N \left(\|\text{ReLU}(g(\mathcal{N}_x(\mathbf{p}_i; \boldsymbol{\theta}), \mathbf{p}_i))\|_1 + \|h(\mathcal{N}_x(\mathbf{p}_i; \boldsymbol{\theta}), \mathbf{p}_i)\|_1 \right),$$

are evaluated for $N = 256$ values of p with corresponding optimal solution \mathbf{x}^* and their values are given in Table 3.

5.1 Linear programming

We use the linear programming example from (De Marchi et al. 2023)

$$\begin{aligned} & \min_{\mathbf{x}} [-0.1 \quad -0.25] \mathbf{x} \\ & \text{s. t. } \begin{bmatrix} 0.01 & 0.01 \\ 0.04 & 0.12 \\ 0.06 & 0.12 \\ -0.1 & 0 \\ 0 & -0.1 \end{bmatrix} \mathbf{x} \leq \begin{bmatrix} 0.4 \\ 2.4 + \frac{p}{1000} \\ 3.12 \\ 0 \\ 0 \end{bmatrix}, \end{aligned}$$

for which the solution can be given in a closed form by

$$(\mathbf{x}^*(p)^\top, \boldsymbol{\mu}^*(p)^\top) = \begin{cases} ((0 \ 26), (0 \ 0 \ 2.0833 \ 0.25 \ 0)), & \text{if } 720 \leq p, \\ ((36 - \frac{p}{20} \ 8 + \frac{p}{40}), (0 \ 1.25 \ 0.833 \ 0 \ 0)), & \text{if } 160 \leq p < 720, \\ ((30 - \frac{p}{80} \ 10 + \frac{p}{80}), (2.5 \ 1.875 \ 0 \ 0 \ 0)), & \text{if } -800 \leq p < 160, \\ ((60 + \frac{p}{40} \ 0), (0 \ 2.5 \ 0 \ 0 \ 0.5)), & \text{if } -2400 \leq p < -800, \\ \text{empty feasible set,} & \text{if } p < -2400. \end{cases}$$

In comparison to (De Marchi et al. 2023), the cost and constraints were rescaled to improve numerical stability. The ranges given here correspond to the neighborhoods of parameter values as defined in Section 2.2, giving $\bar{\mathcal{P}} = \{p \in \mathbb{R} \mid -2400 \leq p \leq 720\}$. In these ranges, the dual variables are constant. For each of these neighborhoods one value was chosen for training, giving four training data points $p_i \in \{-1500, -300, 400, 1500\}$ in total.

Figure 4 shows the results for training an OptINN and a PMNN on this problem using the four data points and an OptINN using no data points for reference. The hyperparameters are shown in Tables 4, 5, and 6.

All three models are able to learn the problem structure well. While the PMNN learns a better representation of the primal variables around the switching points of the active set, we find that both the PMNN and the OptINNs match the ground truth well, even though the OptINNs have in the input and hidden layers the same amount of trainable parameters as the PMNN. All models show a low variance in the results over the five different seeds. While the PMNN better fits the primal variables, the OptINNs better abide by the constraints. For the OptINNs, we observe a smoothing effect around the switching of the active constraint. This smoothing effect likely results from imperfect enforcement of complementary slackness, leading to non-zero dual variables near constraint transitions.

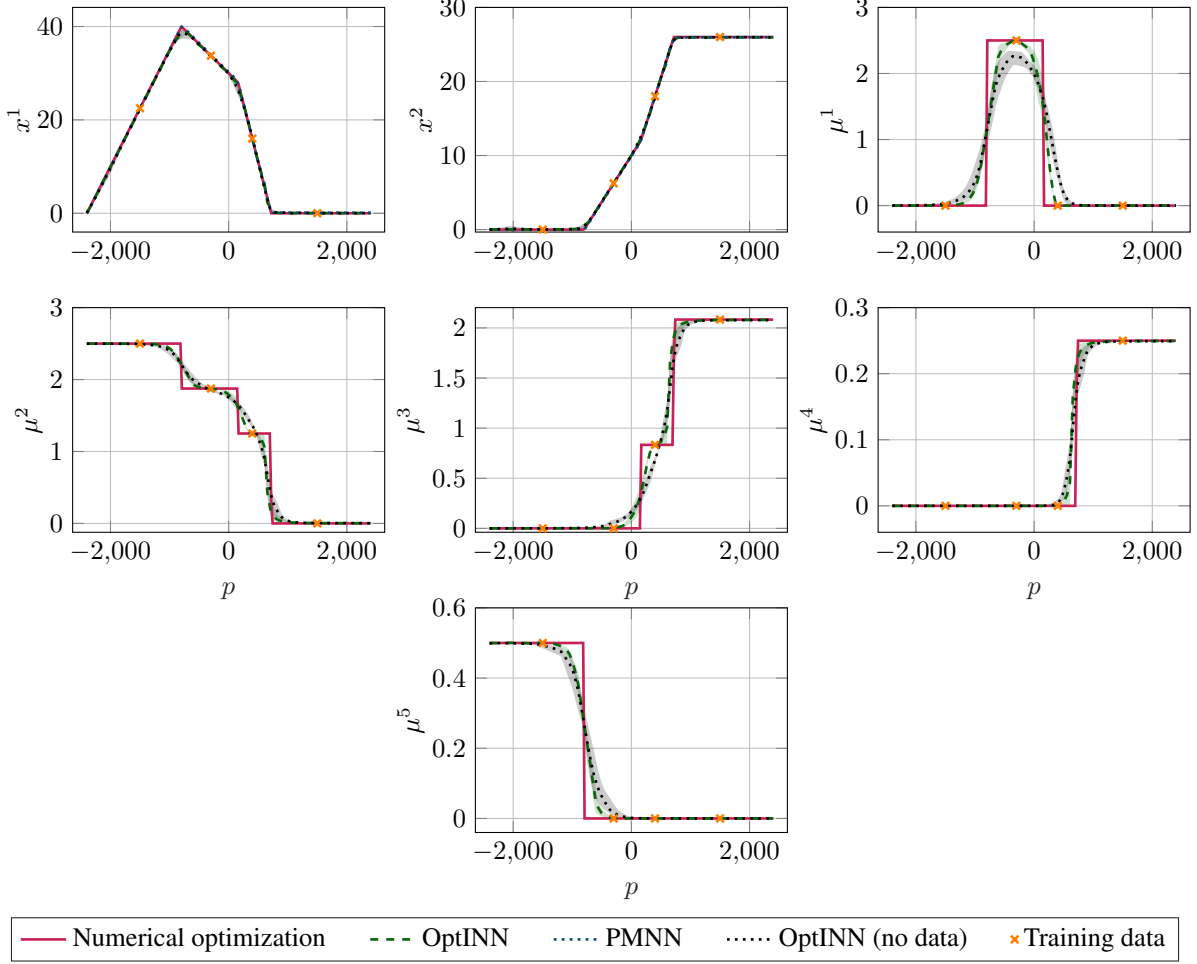


Figure 4 Comparison of the training results for a quadratic-penalty-method-based NN (PMNN) and two OptINN using four and no data points. Displayed are the mean (line) and the area between the minimum and maximum (shaded) for all three methods over five trainings. We observe for all methods a good tracking of the primal-variables. While the OptINNs exhibits a larger spread along jumps in the dual variables, they are able to give reasonable estimations

Figure 5 shows the training curves for both, the OptINN trained with four data points and the OptINN trained without data points. We find that including data points leads to a faster convergence, lower values at earlier epochs, with better, i.e. lower, final values for both the data-based validation loss and the KKT-loss. Still, the good performance of the data-free training (see Table 3) indicates that the optimality-informed loss is able to guide the training well.

5.2 Nonconvex inequality constraints

Given the polynomial $f(x) = 2x^3 + 3x^2 + 2x + 1$ and the parameter region of interest $\bar{\mathcal{P}} = \{\mathbf{p} \in \mathbb{R}^2 \mid \|\mathbf{p}\|_\infty \leq 1\}$, the objective of the second example is to find the point $\mathbf{z} = [z_1 \ z_2]^\top \in \mathbb{R}^2$ closest to the target point $\mathbf{p} \in \mathbb{R}^2$, while \mathbf{z} is subject to four non-convex constraints, giving the optimization problem

$$\begin{aligned} & \min_{\mathbf{z} \in \mathbb{R}^2} \|\mathbf{z} - \mathbf{p}\|_2^2 \\ & \text{s. t. } z_2 \leq f(z_1) \\ & \quad -z_2 \leq f(z_1) \\ & \quad z_2 \leq f(-z_1) \\ & \quad -z_2 \leq f(-z_1). \end{aligned}$$

The constraints are shown in Figure 6, \mathbf{z} is constrained to remain inside of them. If the target value \mathbf{p} satisfies the constraints itself, the optimal solution $\mathbf{z}^* = \mathbf{p}$, otherwise \mathbf{z}^* will lie on the closest constraint such that the vector from

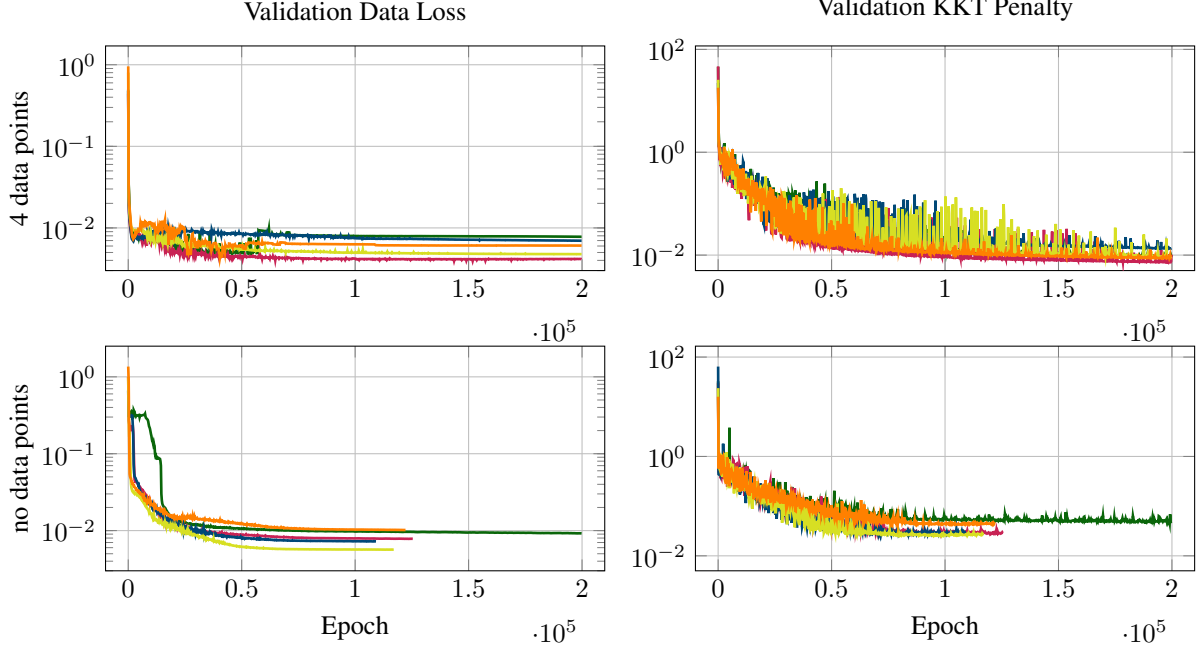


Figure 5 Training curves for both, OptINNs trained with 4 data points (top row) and without data points (bottom row). The left column shows the data-based validation loss (256 validation data points), the right column the KKT-loss. Each color corresponds to a training with different random seed. The validation data were not used for any decision making during training, we included them purely for evaluation. The 4 of the 5 training runs terminate since no improvement was made for 20000 epochs. For both trainings, we do not observe any overfitting, i.e. there is not any increase in the validation data loss

\mathbf{z}^* to \mathbf{p} is perpendicular to the corresponding constraint’s tangent. For both the training of a PMNN and an OptINN, the figure shows the training input data, test input data and test prediction. Again, we find that both methods are able to learn the overall structure of the problem’s solution, indicated by large differences between \mathbf{z}^* and \mathbf{p} outside and small differences inside of the constraints.

Being inferior in both metrics, the OptINN still has a similar performance to the PMNN, while giving estimates for the dual variables as well.

5.3 Linear optimal control problem – Rocket car

Next, we show the learning results for the optimal control of the rocket car, a simple double integrator given by $\ddot{z}(t) = u(t)$. Here, we employ full discretization, a direct optimal control method, where $\mathbf{x} = [z, v]^\top \in \mathbb{R}^2$ denotes the system’s state and the acceleration $u \in \mathbb{R}$ the input to the system. Discretization of the ODE into $N = 32$ time steps, with $\Delta t = \frac{t_f}{N} = 0.4$ s, using the zero-order hold condition (fixed input u for the length of one time step) gives the finite-dimensional optimization problem

$$\begin{aligned}
& \min_{\mathbf{x}, u} \Delta t \sum_{k=0}^{N-1} u[k]^2 \\
& \text{s. t. } \mathbf{x}[k+1] = \begin{bmatrix} 1 & \Delta t \\ 0 & 1 \end{bmatrix} \mathbf{x}[k] + \begin{bmatrix} \frac{\Delta t^2}{2} \\ \Delta t \end{bmatrix} u[k] \quad \forall k \in \{0, \dots, N-1\} \\
& \mathbf{x}[0] = \begin{bmatrix} 0 \\ 0 \end{bmatrix} \\
& \mathbf{x}[N-1] = \begin{bmatrix} p \\ 0 \end{bmatrix} \\
& -1 \leq u[k] \leq 1 \quad \forall k \in \{0, \dots, N-1\},
\end{aligned}$$

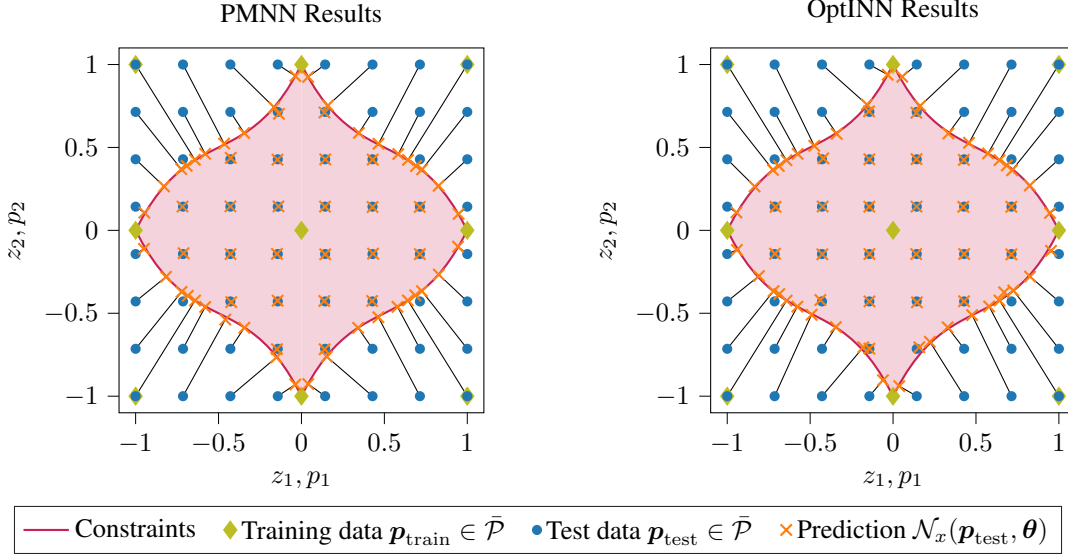


Figure 6 Comparison of OptINN and Penalty-method-based NN results for the quadratic problem with non-convex constraints. The MLP is not able to learn any meaningful representation due to missing information on constraints. The OptINN learned that for \mathbf{p} outside of the constraints large changes are necessary and for \mathbf{p} inside of the constraints the results are much closer to an identity mapping. Moreover, the vector between \mathbf{p} and \mathbf{z} is perpendicular on the corresponding constraint’s tangent as predicted to be optimal

where $\cdot[k]$ indicates the discretized quantity at the k -th point in time $t_k = k\Delta t$. The terminal position $p \in \bar{\mathcal{P}} = \{p \in \mathbb{R} \mid 0 \leq p \leq 40\}$ is the parameter in this problem, giving $n_x = 98$, $n_p = 1$, $n_g = 64$, and $n_h = 68$. For more information regarding optimal control refer to (Gerds 2012).

For this experiment we used three parameter values $p_i \in \{0, 20, 40\}$ for generating training data. These values no longer form a valid set of samples to cover $\bar{\mathcal{P}}$ for Assumption 2, as for values of $p \geq 28.16$ entries of the increasing input u will be constrained by the boundary constraints, leading to an increasing amount of active inequality constraints for increasing p . Since, except for $p = 40$, these cases are not part of the training data, the PMNN and OptINN have to learn the activity of the constraints from the constraint-penalizing and KKT-loss, respectively. The accuracy of the OptINN and PMNN can be evaluated using Figure 7 where for each of the decision variables (position z , velocity v , and acceleration u) heatmaps of the deviation from optimization results using IPOPT and CasADi are shown. Both methods clearly learn beyond a memorization of the training data, indicated by generally low errors. As predicted, the errors increase around $p = 28$, with the OptINN showing lower errors.

Figure 8 shows the results for $p = 38$, the value with the highest deviation between OptINN prediction (but not PMNN prediction) and ground truth. Both methods generally follow the ground truth well, however, even at its worst-performing input value, the OptINN produces lower errors than the PMNN, especially regarding acceleration.

The mean, minimum, and maximum difference between ground truth and prediction for the primal variables of all five trainings is shown in Figure 9 over the parameter values from 0 to 40. We find that the OptINN produces lower errors over the almost the entire range. The most prominent difference between PMNN and OptINN is the prediction capabilities around training data. While the error between the $p = 0$ and $p = 20$ is not visible for the OptINN, the PMNN error promptly jumps to larger values. A similar effect can be observed between $p = 20$ and $p = 40$, where the PMNN error increases abruptly around $p = 20$, while the OptINN error increases slowly over the parameter. Due to the trivialization layer, the OptINN satisfies the box constraints on u everywhere.

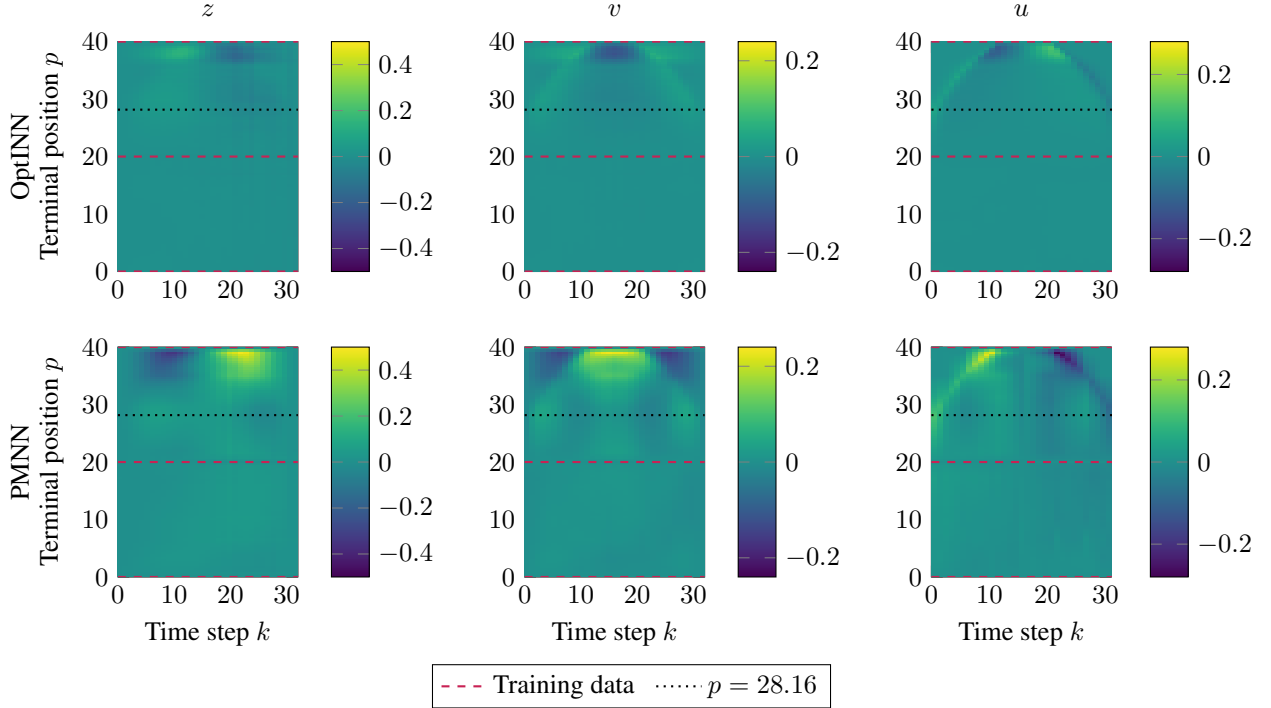


Figure 7 Rocket car: Heatmap of the (signed) deviation between ground truth and OptINN prediction, PMNN prediction, respectively, for 101 equidistant values of the terminal position p . The dashed, red lines mark training data. The deviation is overall small, with the largest deviations appearing where u is producing active inequality constraints for values $p \geq 28.16$. Still, at data points and specifically for all p at the terminal condition, the difference is close to zero

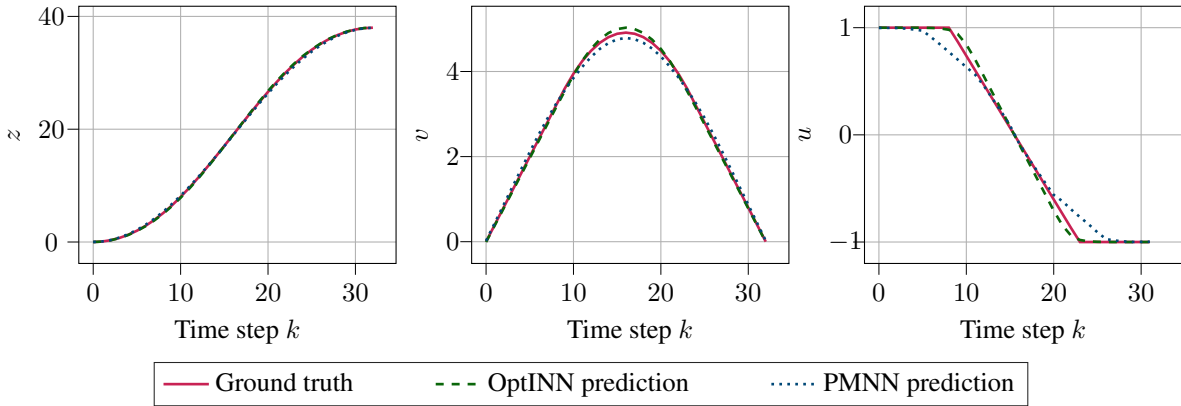


Figure 8 Comparison of the optimal solution (solid) and the OptINN prediction (dashed) for the rocket car optimal control problem with $p = 38$, which was not part of the training data and exhibited the largest deviation to the optimal solution for the OptINN but not the PMNN. For both models, the terminal position is reached, the OptINN produces smaller deviations from ground truth, especially in the acceleration u

5.4 Nonlinear optimal control problem – Pendulum swing-up

Finally, we aim to solve the classical control problem of swinging up a pendulum by application of torque. The system is described by a nonlinear ODE $ml^2\ddot{\varphi} = \tau - mgl\sin(\varphi)$, where τ is the applied torque, m is the mass of the weight at the end of the rod, g is the gravitational acceleration, and l is the length of the rod. After introducing the state

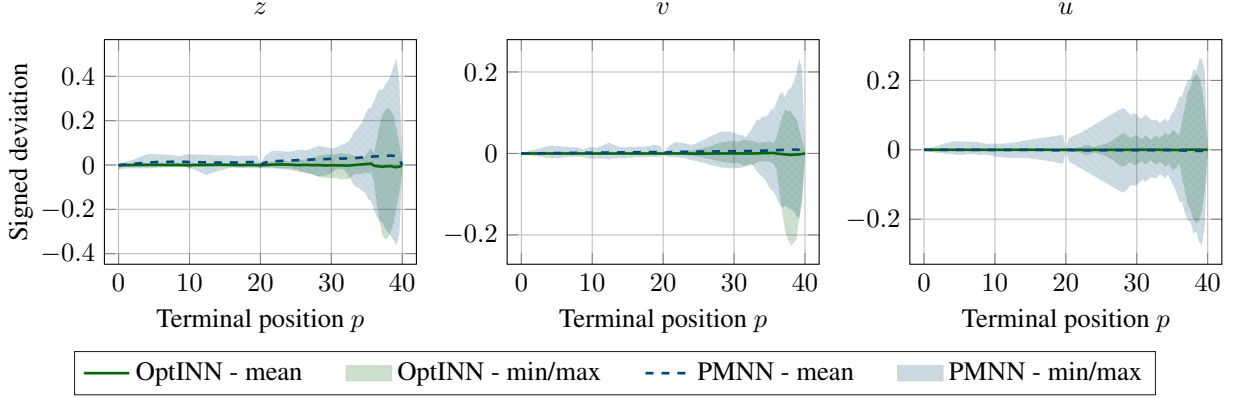


Figure 9 Mean, minimum, and maximum signed deviation from ground truth for both methods over the parameter value. The OptINN produces smaller deviations for most parameters and a significantly lower error over all parameters

representation $\mathbf{x} = [\varphi, \dot{\varphi}]^\top$, the corresponding optimal control problem is

$$\begin{aligned} & \min_{\tau(t)} \int_0^p \tau(t)^2 dt \\ & \text{s. t. } \dot{\mathbf{x}}(t) = \begin{bmatrix} x_2(t) \\ -\frac{g}{l} \sin(x_1(t)) \end{bmatrix} + \begin{bmatrix} 0 \\ \frac{\tau(t)}{ml^2} \end{bmatrix} \\ & \mathbf{x}(0) = \begin{bmatrix} 0 \\ 0 \end{bmatrix} \\ & \mathbf{x}(p) = \begin{bmatrix} \pi \\ 0 \end{bmatrix} \\ & -2 \leq \tau(t) \leq 2. \end{aligned}$$

As there exists no exact discretization, unlike in the previous example, we will use the classical Runge-Kutta method of order 4 (RK4) (cf. (Gerds 2012)). For the resulting optimization problem

$$\begin{aligned} & \min_{\mathbf{x}, u} \Delta t(p) \sum_{k=0}^{N-1} \tau[k]^2 \\ & \text{s. t. } \mathbf{x}[k+1] = \text{RK4}(\mathbf{x}[k], \tau[k], \Delta t(p)) \quad \forall k \in \{0, \dots, N-1\} \\ & \mathbf{x}[0] = \begin{bmatrix} 0 \\ 0 \end{bmatrix} \\ & \mathbf{x}[N] = \begin{bmatrix} \pi \\ 0 \end{bmatrix} \\ & -2 \leq \tau[k] \leq 2 \quad \forall k \in \{0, \dots, N-1\}. \end{aligned}$$

the time step $\Delta t(p) = \frac{p}{N}$ depends on the parameter $p \in \bar{\mathcal{P}} = \{p \in \mathbb{R} \mid 6 \leq p \leq 15\}$, the time to reach the upright position. Here, instead of using constraints, we fix $\mathbf{x}[0]$ and $\mathbf{x}[N]$ to their corresponding values, reducing the number of equality constraints by 4. With $N = 100$, this problem has $n_x = 298$, $n_p = 1$, $n_g = 200$, and $n_h = 200$. This formulation corresponds to an epsilon-constraint scalarization (see for example (Marler and Arora 2004)) of the multi-objective optimal control problem seeking optimal trade-offs between minimum energy consumption and shortest transition time.

Unlike the previous linear-quadratic (and with that convex) problem, the swing-up of the pendulum has multiple local minima. Both the PMNN and OptINN are local methods, so comparing with the ground-truth solution might show large errors for solutions with comparable cost. For that, we compare for both methods how close their predicted costs are to the ground-truth solution and how strongly they violate the equality constraints using the relative and mean absolute error, respectively. We observed no violation of the inequality constraints for both methods. Figure 10 shows the violation of equality constraints (a) and cost of the prediction (b) for a given transition time. The OptINN produces on average a mean absolute constraint violation one magnitude lower than the PMNN. As predicted, the PMNN exhibits

in this example the tendency of the penalty-method to predict solutions outside of the feasible region with costs too low. This explains why the cost of the PMNN prediction appear to be much lower than that of ground-truth or the closely fitting OptINN.

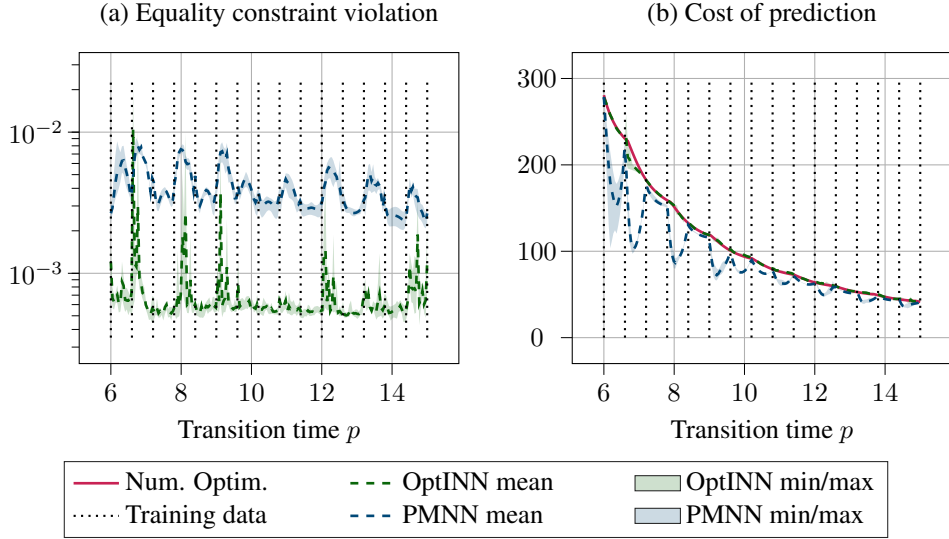


Figure 10 Comparison of PMNN and OptINN on the pendulum swing-up. For most values of p , the means of the absolute values of the constraint violation of all equality constraints in OptINN is one magnitude lower than those from PMNN. Consequently, the cost of the OptINN prediction is much closer to the numerical optimization than the PMNN. Even after hyperparameter optimization, the PMNN shows the tendency of the quadratic-penalty method to underestimate costs and predict solutions outside of the feasible region

Table 3 Summary of numerical evaluation metrics. The value shown is the mean over all parameter values and all five validation trainings

Problem	Method	Error Metric ↓	Eq. Violation ↓	Ineq. Violation ↓
<i>Metric: Primal MSE</i>				
Lin. Prog.	PMNN	1.61×10^{-2}	–	4.8×10^{-4}
	OptINN	3.30×10^{-2}	–	6.01×10^{-5}
	OptINN (no data)	1.03×10^{-1}	–	1.55×10^{-5}
Nonconvex	PMNN	5.98×10^{-5}	–	1.67×10^{-4}
	OptINN	4.07×10^{-4}	–	2.38×10^{-4}
Rocket car	PMNN	2.34×10^{-3}	3.8×10^{-3}	8.55×10^{-7}
	OptINN	5.33×10^{-4}	1.74×10^{-3}	0
<i>Metric: Cost MSE</i>				
Pendulum	PMNN	1.35×10^{-1}	4.04×10^{-3}	5.18×10^{-6}
	OptINN	1.19×10^{-2}	7.26×10^{-4}	0

5.5 Summary

In our numerical experiments on small-scale optimization problems, OptINNs demonstrated performance comparable to PMNNs in predicting primal variables and constraint violations, with the added advantage of providing estimates for dual variables. For larger-scale problems, however, the OptINN clearly outperforms the PMNN across all evaluated metrics.

Inspecting the tables in Appendix A, we observe that the tuned hyperparameters for PMNNs are significantly more extreme than those for OptINNs. Notably, OptINNs consistently support training with higher learning rates. The

disparity is most pronounced in the trade-off parameter α , which balances the data-based loss against the penalty term. While the bounds $\underline{\alpha}$ and $\bar{\alpha}$ for the OptINN span a broad range of moderate magnitude, the PMNN necessitates an increasingly dominant weighting of the data-based loss.

6 Conclusion and outlook

In this work, we proposed Optimality-Informed Neural Networks (OptINNs) to learn the parameter-to-optimal-solution mapping of parametric optimization problems. Unlike previous works that rely primarily on the quadratic-penalty method, we introduced a problem-specific architecture and a loss function rooted in the Karush-Kuhn-Tucker (KKT) conditions. This formulation yields two key advantages: first, it enables the simultaneous prediction of optimal decision variables and the corresponding Lagrange multipliers. Second, unlike data-based validation metrics, the KKT residual can be computed from randomly sampled parameter values, serving as a self-supervised metric. Since the KKT loss is lower-bounded by zero, it is directly applicable for both hyperparameter tuning and model validation without requiring additional ground-truth data. By adopting the perspective of theory-informed deep learning, we leveraged established techniques such as adaptive weight balancing to train these networks to high accuracy even in low-data regimes.

Our numerical experiments across four benchmark problems, linear programming, non-convex constraints, and both linear and nonlinear optimal control, demonstrate the efficacy of the proposed method. For smaller problems, OptINNs achieve a performance comparable to those of penalty-based networks, with the added benefit of predicting dual variables. However, for larger optimal control tasks, OptINNs demonstrate superior performance, achieving lower constraint violations and higher fidelity to numerical solvers. We attribute this superiority to the explicit KKT guidance, which avoids the known tendency of quadratic-penalty methods to converge towards infeasible local minima.

The methodological framework presented here is model-agnostic and can be generalized to other parametric models. Currently, the reliance on Multi-Layer Perceptrons restricts OptINNs to optimization problems with fixed dimensionality. Future research should therefore investigate dynamic architectures, such as Recurrent Neural Networks or Transformers, to mitigate this restriction and accommodate variable-sized problem instances.

Furthermore, several directions remain for improving training efficiency and applicability. Using penalty-based methods for pretraining OptINNs could significantly accelerate early convergence. Regarding applications, the rapid inference capabilities of OptINNs make them highly suitable for real-time optimal control; their integration into Model Predictive Control workflows warrants further study. Additionally, exploiting parametric sensitivity analysis offers a promising avenue for data efficiency. Computing the derivatives of optimal solutions with respect to problem parameters would enable Sobolev training, extracting richer gradient information from the available training data. Finally, to strengthen the theoretical foundations, future work should investigate the alignment of this problem setting with the field of tame optimization to establish convergence properties.

Statements and Declarations

None

References

- Akiba, Takuya et al. (2019). “Optuna: A Next-generation Hyperparameter Optimization Framework”. In: *Proceedings of the 25th ACM SIGKDD International Conference on Knowledge Discovery & Data Mining*. KDD ’19. Anchorage, AK, USA: Association for Computing Machinery, 2623–2631. DOI: <https://doi.org/10.1145/3292500.3330701>.
- Allgower, Eugene L and Kurt Georg (1990). *Numerical Continuation Methods: an Introduction*. Springer. DOI: <https://doi.org/10.2307/2153001>.
- Andersson, Joel A. E. et al. (2019). “CasADi: a software framework for nonlinear optimization and optimal control”. In: *Math. Program. Comput.* 11, pp. 1–36. DOI: <https://doi.org/10.5281/zenodo.1257968>.
- Ba, Jimmy Lei, Jamie Ryan Kiros, and Geoffrey E. Hinton (2016). *Layer Normalization*. DOI: <https://doi.org/10.48550/ARXIV.1607.06450>.
- Barron, A.R. (1993). “Universal approximation bounds for superpositions of a sigmoidal function”. In: *IEEE Trans. Inf. Theory* 39.3, 930–945. DOI: <https://doi.org/10.1109/18.256500>.
- Bemporad, Alberto et al. (2002). “The explicit linear quadratic regulator for constrained systems”. In: *Automatica* 38.1, pp. 3–20. DOI: [https://doi.org/10.1016/S0005-1098\(01\)00174-1](https://doi.org/10.1016/S0005-1098(01)00174-1).
- Bengio, Yoshua, Olivier Delalleau, and Nicolas Roux (2005). “The Curse of Highly Variable Functions for Local Kernel Machines”. In: *Advances in Neural Information Processing Systems*. Ed. by Y. Weiss, B. Schölkopf, and J. Platt. Vol. 18. MIT Press.
- Bergstra, James et al. (2011). “Algorithms for Hyper-Parameter Optimization”. In: *Advances in Neural Information Processing Systems*. Ed. by J. Shawe-Taylor et al. Vol. 24. Curran Associates, Inc.
- Berzins, Arturs et al. (2024). “Geometry-Informed Neural Networks”. In: *arXiv preprint arXiv:2402.14009*. DOI: <https://doi.org/10.48550/arXiv.2402.14009>.
- Bishop, Christopher M and Hugh Bishop (2023). *Deep learning: Foundations and concepts*. Springer Nature. DOI: <https://doi.org/10.1007/978-3-031-45468-4>.
- Boyd, Stephen and Lieven Vandenbergh (2004). *Convex optimization*. Cambridge University Press. DOI: <https://doi.org/10.1017/cbo9780511804441>.
- Büskens, Christof and Dennis Wassel (2013). “The ESA NLP Solver WORHP”. In: *Modeling and Optimization in Space Engineering*. Ed. by Giorgio Fasano and János D. Pintér. Vol. 73. Springer New York, pp. 85–110. DOI: https://doi.org/10.1007/978-1-4614-4469-5_4.
- Chen, Ricky T. Q. et al. (2018). “Neural Ordinary Differential Equations”. In: *Advances in Neural Information Processing Systems*. Ed. by S. Bengio et al. Vol. 31. Curran Associates, Inc.
- Cheng, Tao, Frank L. Lewis, and Murad Abu-Khalaf (2005). “Nearly optimal control laws for nonlinear systems with saturating actuators using a neural network HJB approach”. In: *Automatica* 41.5, pp. 779–791. DOI: <https://doi.org/10.1016/j.automatica.2004.11.034>.
- De Marchi, Alberto et al. (2023). “A Function Approximation Approach for Parametric Optimization”. In: *J. Optim. Theory Appl.* 196.1, pp. 56–77. DOI: <https://doi.org/10.1007/S10957-022-02138-4>.
- Dhingra, A. K. and S. S. Rao (1992). “A neural network based approach to mechanical design optimization”. In: *Eng. Optimiz.* 20.3, pp. 187–203. DOI: <https://doi.org/10.1080/03052159208941280>.
- Effati, Sohrab and Morteza Pakdaman (2013). “Optimal control problem via neural networks”. In: *Neural Computing and Applications* 23.7, pp. 2093–2100. DOI: <https://doi.org/10.1007/s00521-012-1156-2>.
- Fiacco, Anthony V. (1983). *Introduction To Sensitivity And Stability Analysis In Nonlinear Programming*. Vol. 165. Mathematics in Science and Engineering. New York: Academic Press.
- Gerds, Matthias (2012). *Optimal Control of ODEs and DAEs*. Berlin, Boston: De Gruyter. DOI: <https://doi.org/10.1515/9783110249996>.
- Goodfellow, Ian, Yoshua Bengio, and Aaron Courville (2016). *Deep Learning*. MIT Press.
- Guddat, J., F. Guerra Vazquez, and H. Th. Jongen (1990). *Parametric Optimization: Singularities, Pathfollowing and Jumps*. Vieweg+Teubner Verlag. DOI: <https://doi.org/10.1007/978-3-663-12160-2>.
- Hopfield, John J. and David W. Tank (1985). ““Neural” computation of decisions in optimization problems”. In: *Biol. Cybern.* 52.3, pp. 141–152. DOI: <https://doi.org/10.1007/BF00339943>.
- Izzo, Dario, Ekin Öztürk, and Marcus Mörtens (2019). “Interplanetary transfers via deep representations of the optimal policy and/or of the value function”. In: *Proceedings of the Genetic and Evolutionary Computation Conference Companion*. GECCO ’19. Prague, Czech Republic: Association for Computing Machinery, 1971–1979. DOI: <https://doi.org/10.1145/3319619.3326834>.
- Krishnapriyan, Aditi et al. (2021). “Characterizing possible failure modes in physics-informed neural networks”. In: *Advances in neural information processing systems* 34, pp. 26548–26560.
- Lange, Kenneth (2013). “Penalty and Barrier Methods”. In: *Optimization*. New York, NY: Springer New York. Chap. 13, pp. 313–339. DOI: https://doi.org/10.1007/978-1-4614-5838-8_13.
- Lillo, W.E. et al. (1993). “On solving constrained optimization problems with neural networks: a penalty method approach”. In: *IEEE Trans. Neural Netw.* 4.6, 931–940. DOI: <https://doi.org/10.1109/72.286888>.

- Liu, Xinran et al. (2024). “Teaching Networks to Solve Optimization Problems”. In: *IEEE Access* 12, pp. 17102–17113. DOI: <https://doi.org/10.1109/ACCESS.2024.3358724>.
- Loshchilov, Ilya and Frank Hutter (2019). “Decoupled Weight Decay Regularization”. In: *International Conference on Learning Representations*.
- Markowitz, Harry (1952). “Portfolio Selection”. In: *J. Finance* 7.1, 77–91. DOI: <https://doi.org/10.1111/j.1540-6261.1952.tb01525.x>.
- Marler, R Timothy and Jasbir S Arora (2004). “Survey of multi-objective optimization methods for engineering”. In: *Structural and multidisciplinary optimization* 26.6, pp. 369–395. DOI: <https://doi.org/10.1007/s00158-003-0368-6>.
- Martins, Joaquim R. R. A. and Andrew Ning (2021). *Engineering design optimization*. Cambridge University Press. DOI: <https://doi.org/10.1017/9781108980647>.
- Munos, R., L. C. Baird, and A. W. Moore (1999). “Gradient descent approaches to neural-net-based solutions of the Hamilton-Jacobi-Bellman equation”. In: *IJCNN’99. International Joint Conference on Neural Networks. Proceedings (Cat. No.99CH36339)*. Vol. 3, 2152–2157 vol.3. DOI: <https://doi.org/10.1109/IJCNN.1999.832721>.
- Nakamura-Zimmerer, Tenavi, Qi Gong, and Wei Kang (2021). “Adaptive Deep Learning for High-Dimensional Hamilton-Jacobi-Bellman Equations”. en. In: *SIAM J. Sci. Comput.* 43.2, A1221–A1247. DOI: <https://doi.org/10.1137/19M1288802>.
- Nikbakht, Rasoul, Anders Jonsson, and Angel Lozano (2020). “Unsupervised learning for parametric optimization”. In: *IEEE Commun. Lett.* 25.3, pp. 678–681. DOI: <https://doi.org/10.1109/LCOMM.2020.3027981>.
- Nocedal, Jorge and Stephen J. Wright (2006). *Numerical Optimization*. Springer Series in Operations Research and Financial Engineering. Springer New York, NY. DOI: <https://doi.org/10.1007/978-0-387-40065-5>.
- Oberdieck, Richard et al. (2016). “On multi-parametric programming and its applications in process systems engineering”. In: *Chem. Eng. Res. Des.* 116, 61–82. DOI: <https://doi.org/10.1016/j.cherd.2016.09.034>.
- Paszke, Adam et al. (2019). “PyTorch: An Imperative Style, High-Performance Deep Learning Library”. In: *Advances in Neural Information Processing Systems*. Ed. by H. Wallach et al. Vol. 32. Curran Associates, Inc.
- Raissi, M., P. Perdikaris, and G.E. Karniadakis (2019). “Physics-informed neural networks: A deep learning framework for solving forward and inverse problems involving nonlinear partial differential equations”. en. In: *J. Comput. Phys.* 378, pp. 686–707. DOI: <https://doi.org/10.1016/j.jcp.2018.10.045>.
- Rao, J. R. J. and P. Y. Papalambros (1989a). “A nonlinear programming continuation strategy for one parameter design optimization problems”. In: *International Design Engineering Technical Conferences and Computers and Information in Engineering Conference*. Vol. 3684. American Society of Mechanical Engineers, pp. 77–89. DOI: <https://doi.org/10.1115/detc1989-0077>.
- Rao, J. R. J. and P. Y. Papalambros (1989b). “Extremal Behavior of One Parameter Families of Optimal Design Models”. In: *15th Design Automation Conference: Volume 2 — Design Optimization*. DETC89. American Society of Mechanical Engineers, 91–100. DOI: <https://doi.org/10.1115/detc1989-0078>.
- Rheinboldt, Werner C. (1988). “On the computation of multi-dimensional solution manifolds of parametrized equations”. In: *Numer. Math.* 53.1, pp. 165–181. DOI: <https://doi.org/10.1007/bf01395883>.
- Rivas, Alberto et al. (2020). “A predictive maintenance model using recurrent neural networks”. In: *14th International Conference on Soft Computing Models in Industrial and Environmental Applications (SOCO 2019) Seville, Spain, May 13–15, 2019, Proceedings 14*. Springer, pp. 261–270. DOI: https://doi.org/10.1007/978-3-030-20055-8_25.
- Seo, Jaemin (2024). “Solving real-world optimization tasks using physics-informed neural computing”. en. In: *Sci. Rep.* 14.1, p. 202. DOI: <https://doi.org/10.1038/s41598-023-49977-3>.
- Sirignano, Justin and Konstantinos Spiliopoulos (2018). “DGM: A deep learning algorithm for solving partial differential equations”. In: *J. Comput. Phys.* 375, pp. 1339–1364. DOI: <https://doi.org/10.1016/j.jcp.2018.08.029>.
- Verma, Deepanshu et al. (2024). *Neural Network Approaches for Parameterized Optimal Control*. DOI: <https://doi.org/10.48550/ARXIV.2402.10033>.
- Wächter, Andreas and Lorenz T. Biegler (2006). “On the implementation of an interior-point filter line-search algorithm for large-scale nonlinear programming”. In: *Mathematical programming* 106, pp. 25–57. DOI: <https://doi.org/10.1007/s10107-004-0559-y>.
- Wang, Sifan et al. (2023). *An Expert’s Guide to Training Physics-informed Neural Networks*. en.
- Wu, A. I. and P. K. S. Tam (1999). “A neural network methodology of quadratic optimization”. In: *Int. J. Neural Syst.* 09.02, pp. 87–93. DOI: <https://doi.org/10.1142/S0129065799000083>.
- Zhang, Shengwei and A. G. Constantinides (1992). “Lagrange programming neural networks”. In: *IEEE Trans. Circuits Syst. II* 39.7, pp. 441–452. DOI: <https://doi.org/10.1109/82.160169>.

Appendix

A Hyperparameters for numerical examples

Here, we summarize the hyperparameters used for training Optimality-informed (OptINN) and quadratic-penalty-method-based neural networks (PMNN) in the numerical examples. The depth describes the number of hidden layers, excluding input, output and trivialization layer. The width is the number of neurons in each hidden layer. The learning rate (LR) is the initial learning rate used in the AdamW optimizer (Loshchilov and Hutter 2019) with default parameters, using a learning rate scheduler (ReduceLRonPlateau) that reduces the learning rate by a factor of 0.8 if the validation loss does not improve for 2000 epochs. Additionally, the training was early terminated if the validation loss did not improve for 20000 epochs. For OptINNs the validation loss is the KKT-loss \mathcal{L}^{KKT} evaluated on #Validation samples of p with $P^i(x) = |x|, i \in \mathcal{T}$, for PMNNs it is \mathcal{L}^{PM} for fixed γ_g and γ_h . #Data is the number training data and the batch size that were generated in the same way. #Training is the number of p samples (N in the equations) used for the training loss.

Linear programming

Table 4 Hyperparameters for training the OptINN on the optimal control for the linear programming problem.

Epochs	#Data	LR	Width	$\underline{\alpha}$	init. phase	weight decay
$2 \cdot 10^5$	4	$8.58 \cdot 10^{-3}$	50	$1.5 \cdot 10^{-4}$	4,000	$6.39 \cdot 10^{-4}$
#Training	#Validation	β	Depth	$\bar{\alpha}$	final. phase	Penalty type
480	512	$8 \cdot 10^{-3}$	3	$2.4 \cdot 10^{-2}$	$1.24 \cdot 10^5$	3

Table 5 Hyperparameters for training the OptINN on the optimal control for the linear programming problem.

Epochs	#Data	LR	Width	$\underline{\alpha}$	init. phase	weight decay
$2 \cdot 10^5$	4	$8.58 \cdot 10^{-3}$	50	1	4,000	$6.39 \cdot 10^{-4}$
#Training	#Validation	β	Depth	$\bar{\alpha}$	final. phase	Penalty type
480	512	$8 \cdot 10^{-3}$	3	1	$1.24 \cdot 10^5$	3

Table 6 Hyperparameters for training the PMNN on the linear programming problem.

Epochs	#Data	Width	LR	γ_g
$2 \cdot 10^5$	4	50	$9.61 \cdot 10^{-3}$	656.23
#Training	#Validation	Depth	α	γ_h
950	512	3	$3.99 \cdot 10^{-2}$	0

Nonconvex inequality constraints

Table 7 Hyperparameters for training the OptINN on the problem with nonconvex inequality constraints.

Epochs	#Data	LR	Width	$\underline{\alpha}$	init. phase	weight decay
$2 \cdot 10^5$	9	$1.2 \cdot 10^{-2}$	40	$7.81 \cdot 10^{-5}$	23,000	$2.16 \cdot 10^{-3}$
#Training	#Validation	β	Depth	$\bar{\alpha}$	final. phase	Penalty type
500	512	$5 \cdot 10^{-3}$	5	$2.22 \cdot 10^{-3}$	72,000	4

Table 8 Hyperparameters for training the PMNN on the problem with nonconvex inequality constraints.

Epochs	#Data	Width	LR	γ_g
$2 \cdot 10^5$	9	40	$2.5 \cdot 10^{-3}$	1,176.53
#Training	#Validation	Depth	α	γ_h
990	512	5	0.38	0

Linear optimal control problem – Rocket car**Table 9** Hyperparameters for training the OptINN on the optimal control for the rocket car.

Epochs	#Data	LR	Width	$\underline{\alpha}$	init. phase	weight decay
$2 \cdot 10^5$	3	$1.77 \cdot 10^{-3}$	400	$1.2 \cdot 10^{-2}$	31,000	$8.53 \cdot 10^{-5}$
#Training	#Validation	β	Depth	$\bar{\alpha}$	final. phase	Penalty type
380	512	$5 \cdot 10^{-3}$	5	0.73	70,000	2

Table 10 Hyperparameters for training the PMNN on the optimal control for the rocket car.

Epochs	#Data	Width	LR	γ_g
$2 \cdot 10^5$	3	400	$8.82 \cdot 10^{-4}$	$1.38 \cdot 10^5$
#Training	#Validation	Depth	α	γ_h
360	512	5	$8.79 \cdot 10^{-5}$	182.7

Nonlinear optimal control problem – Pendulum swing-up**Table 11** Hyperparameters for training the OptINN on the optimal control for the pendulum.

Epochs	#Data	LR	Width	$\underline{\alpha}$	init. phase	weight decay
$2 \cdot 10^5$	16	$1.45 \cdot 10^{-3}$	800	$1.99 \cdot 10^{-4}$	2,000	$1.77 \cdot 10^{-4}$
#Training	#Validation	β	Depth	$\bar{\alpha}$	final. phase	Penalty type
560	512	$5 \cdot 10^{-3}$	4	$7.59 \cdot 10^{-2}$	$1.71 \cdot 10^5$	4

Table 12 Hyperparameters for training the PMNN on the optimal control for the pendulum.

Epochs	#Data	Width	LR	γ_g
$2 \cdot 10^5$	16	800	$1.77 \cdot 10^{-4}$	18.36
#Training	#Validation	Depth	α	γ_h
450	512	4	$4.74 \cdot 10^{-6}$	4,039.97

B Proof of Lemma 3.1

If the conditions $\text{KKT}(\mathbf{p})$ are satisfied, it follows that for all $i \in \{1, \dots, n_x\}$, $j \in \{1, \dots, n_h\}$, and $k \in \{1, \dots, n_g\}$

$$\frac{\partial L}{\partial x^i}(\mathbf{x}^*, \boldsymbol{\lambda}^*, \boldsymbol{\mu}^*, \mathbf{p}) = \mathbf{h}^j(\mathbf{x}^*, \mathbf{p}) = \text{ReLU}(\mathbf{g}^k(\mathbf{x}^*, \mathbf{p})) = \boldsymbol{\mu}^k \mathbf{g}^k(\mathbf{x}^*, \mathbf{p}) = 0.$$

From Definition 3.1, since $P^i(0) = 0$, $i \in \mathcal{T}$, it follows that

$$\mathcal{D}^{\text{Stat}}(\mathbf{x}^*, \boldsymbol{\lambda}^*, \boldsymbol{\mu}^*, \mathbf{p}) = \mathcal{D}^{\text{FeasG}}(\mathbf{x}^*, \mathbf{p}) = \mathcal{D}^{\text{FeasH}}(\mathbf{x}^*, \mathbf{p}) = \mathcal{D}^{\text{CSl}}(\mathbf{x}^*, \boldsymbol{\mu}^*, \mathbf{p}) = 0,$$

i.e. KKT-points result in a KKT-loss of 0.

Moreover, assume there exists $(\tilde{\mathbf{x}}, \tilde{\boldsymbol{\lambda}}, \tilde{\boldsymbol{\mu}}) \in \mathbb{R}^{n_x} \times \mathbb{R}^{n_h} \times \mathbb{R}_{\geq 0}^{n_g}$ and $\mathbf{p} \in \mathbb{R}^{n_p}$ not satisfying $\text{KKT}(\mathbf{p})$, with

$$\mathcal{D}^{\text{Stat}}(\tilde{\mathbf{x}}, \tilde{\boldsymbol{\lambda}}, \tilde{\boldsymbol{\mu}}, \mathbf{p}) = \mathcal{D}^{\text{FeasG}}(\tilde{\mathbf{x}}, \mathbf{p}) = \mathcal{D}^{\text{FeasH}}(\tilde{\mathbf{x}}, \mathbf{p}) = \mathcal{D}^{\text{CSl}}(\tilde{\mathbf{x}}, \tilde{\boldsymbol{\mu}}, \mathbf{p}) = 0.$$

Since $(\tilde{\mathbf{x}}, \tilde{\boldsymbol{\lambda}}, \tilde{\boldsymbol{\mu}})$ do not satisfy $\text{KKT}(\mathbf{p})$, for at least one $i \in \{1, \dots, n_x\}$, $j \in \{1, \dots, n_h\}$, or $k \in \{1, \dots, n_g\}$ any of the quantities

$$\frac{\partial L}{\partial x^i}(\tilde{\mathbf{x}}, \tilde{\boldsymbol{\lambda}}, \tilde{\boldsymbol{\mu}}, \mathbf{p}), \mathbf{h}^j(\tilde{\mathbf{x}}, \mathbf{p}), \text{ReLU}(\mathbf{g}^k(\tilde{\mathbf{x}}, \mathbf{p})), \boldsymbol{\mu}^k \mathbf{g}^k(\tilde{\mathbf{x}}, \mathbf{p}),$$

is not equal to 0. This contradicts the assumption that the P^i are unimodal penalty functions, since $P^i(x) = 0$ only at $x = 0$ and $P^i(x) > 0$ everywhere else.